Inorganic Chemistry

Article

pubs.acs.org/IC

Phosphate Ester Bond Hydrolysis Promoted by Lanthanide-Substituted Keggin-type Polyoxometalates Studied by a Combined Experimental and Density Functional Theory Approach

Thi Kim Nga Luong,[†] Tzvetan T. Mihaylov,[‡] Gregory Absillis,[†] Pavletta Shestakova,[§] Kristine Pierloot,[‡] and Tatjana N. Parac-Vogt*[,†]

[†]Laboratory of Bioinorganic Chemistry, Department of Chemistry and [‡]Laboratory of Computational Coordination Chemistry, Department of Chemistry, KU Leuven, Celestijnenlaan 200F, 3001 Leuven, Belgium

[§]NMR Laboratory, Institute of Organic Chemistry with Centre of Phytochemistry, Bulgarian Academy of Sciences, Acad. G. Bontchev Str., B1.9, 1113 Sofia, Bulgaria

Supporting Information

ABSTRACT: Hydrolytic cleavage of 4-nitrophenyl phosphate (NPP), a commonly used DNA model substrate, was examined in the presence of series of lanthanide-substituted Keggin-type polyoxometalates (POMs) $[Me_2NH_2]_{11}[Ce^{III}(PW_{11}O_{39})_2]$, $[Me_2NH_2]_{10}[Ce^{IV}(PW_{11}O_{39})_2]$ (abbreviated as $(Ce^{IV}(PW_{11})_2)$, and $K_4[EuPW_{11}O_{39}]$ by means of NMR and luminescence spectroscopies and density functional theory (DFT) calculations. Among the examined complexes, the Ce(IV)-substituted Keggin POM $(Ce^{IV}(PW_{11})_2)$ showed the highest reactivity, and its aqueous speciation was fully determined under different conditions of pD, temperature, concentration, and ionic strength by means of ^{31}P and ^{31}P diffusion-ordered NMR spectroscopy. The cleavage of the phosphoester bond of NPP in the presence of $(Ce^{IV}(PW_{11})_2)$ proceeded with an observed rate constant $k_{obs} = (5.31 \pm 0.06) \times 10^{-6}$ s^{-1} at pD 6.4 and 50 °C. The pD dependence of NPP hydrolysis exhibits a bell-shaped profile, with the fastest rate observed at pD 6.4. The formation constant ($K_f = 127$ M^{-1}) and catalytic rate constant ($k_c = 19.41 \times 10^{-5}$ s^{-1}) for the NPP-Ce(IV)-Keggin POM complex were calculated, and binding between $Ce^{IV}(PW_{11})_2$ and the phosphate group of NPP was also evidenced by the change of the chemical shift of the ^{31}P nucleus in NPP upon addition of the POM complex. DFT calculations revealed that binding of NPP to the parent catalyst $Ce^{IV}(PW_{11})_2$ is thermodynamically unlikely. On the contrary, formation of complexes with the monomeric 1:1 species, $Ce^{IV}PW_{11}$, is considered to be more favorable, and the most stable complex, $[Ce^{IV}PW_{11}(H_2O)_2(NPP\text{-}\kappa O)_2]^{7-}$, was found to involve two NPP ligands coordinated to the Ce^{IV}center of $Ce^{IV}PW_{11}$ in the monodentate fashion. The formation of such species is considered to be responsible for the hydrolytic activity of $Ce^{IV}(PW_{11})_2$ toward phosphomonoesters. On the basis of these findings a principle mechanism for the hydrolysis of NPP by the POM is proposed.

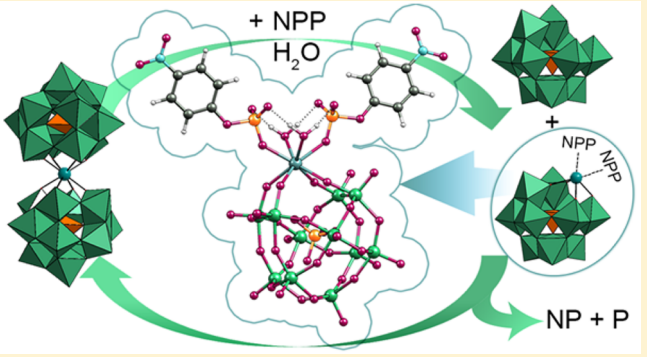

INTRODUCTION

Polyoxometalates (POMs) are oxygen anion clusters of early transition metals (M = V, Nb, Ta, Mo, and W) in their highest oxidation state.[1] They have been known for almost 200 years, since Berzelius discovered the first heteropolyanion compound in 1826.[2] In general, POMs consist of MO_n units, where n (n = 4−7) indicates the coordination number of M. Apart from M and O, other elements, which are usually labeled as X, can be part of the POM framework. As a general rule, they are fourfold or sixfold coordinated and can be found in the center of the M_xO_y shell.[1c,3] The chemically robust nature of POMs, together with their highly tunable physicochemical properties such as acidity, thermal stability, redox potential, solubility, size, shape, and charge, resulted in their application in material science,[4] magnetism,[5] and catalysis.[6] In addition, several classes of POMs have been reported to have potent antitumor, antiviral, and antibacterial properties, resulting in a substantial interest in the potential medicinal application of POMs.[7] To gain deeper insight into their biological activity, we recently examined the reactivity of POMs toward a range of different biologically relevant molecules and their model systems. The incorporation of different transition metal ions with high Lewis acidity into heteropolyoxometalates of the Keggin, Wells−Dawson, and Lindqvist type resulted in catalysts that also displayed reactivity toward hydrolysis of phosphoesters[8] and peptide bonds in peptides and proteins.[9] The Lewis acidic POMs have been also

Received: July 25, 2016

DOI: 10.1021/acs.inorgchem.6b01802
Inorg. Chem. XXXX, XXX, XXX−XXX

used in the past for the transformations of various organic substrates.[10]

Phosphoester bonds form the backbone of DNA and RNA macromolecules and are extremely resistant toward hydrolysis, primarily because of the repulsion between the negatively charged backbone and potential nucleophiles.[11] The half-life for phosphoester bond hydrolysis has been estimated to be ~100 000 years for DNA and 4 years for RNA at neutral pH and 25 °C, in the absence of any catalyst.[12] This stability makes them excellent systems for information storage.[13] Despite the extreme stability of the phosphoester bond, its efficient cleavage is a frequently required procedure in biochemical fields. In nature, phosphatases, a class of enzymes that contains one or more metal ions at the active sites, are responsible for hydrolyzing phosphoester bonds with impressive rate enhancements.[14]

Recently, we reported on the reactivity of early transition metal (Zr(IV) and Hf(IV) substituted Wells−Dawson POMs toward 4-nitrophenylphosphate (NPP) and bis(4-nitrophenyl)-phosphate (BNPP),[8a] revealing that these POMs are able to hydrolyze phosphoester bonds in commonly used DNA model systems. Previous work has shown that due to their high charge density, high coordination number, as well as rapid ligand exchange rates, lanthanide(III) ions are very suitable for designing artificial phosphoesterases. The high reactivity of several lanthanide(III) complexes was demonstrated toward NPP,[15] BNPP,[15,16] 2-hydroxypropyl 4-nitrophenyl phosphate,[16b] 4-nitrophenyl diphenyl phosphate,[16b] DNA, and RNA,[11b,17] demonstraing that lanthanide(III) ions exhibit high affinity for phosphoester bond hydrolysis.[16a,18] In addition, in the lanthanide series Ce(IV) ions have been shown to be the most active toward DNA hydrolysis, presumably due to its high electron-withdrawing activity, high Lewis acidity, high coordination number (up to 12), and fast ligand exchange rate.[19] However, aqueous solutions of Ce(IV) ions are subject to solubility problems at pH > 4, resulting in polymeric metal-hydroxo precipitates. This problem considerably hinders kinetics studies and their application. Therefore, attempts to stabilize Ce(IV) ions by complexation with strong anionic ligands have been made.[20] More recently, we discovered that a Ce(IV)-substituted Keggin POM $[Me_2NH_2]_{11}$-$[Ce^{IV}(PW_{11}O_{39})_2]$, ($Ce^{IV}(PW_{11})_2$), in which the Keggin moiety was used as a chelating agent for Ce(IV), promotes selective peptide bond hydrolysis of hen egg-white lysozyme at physiological pH and temperature and therefore can be regarded as artificial metalloprotease that operates under mild conditions.[21]

This result encouraged us to explore the reactivity of $Ce^{IV}(PW_{11})_2$ toward phosphoester bond hydrolysis in biologically relevant model substrates with the aim to assess the potential phosphoesterase properties of the lanthanide-substituted POMs. For this purpose we choose NPP, which is a commonly used model substrate for biological phosphoesters. In addition, the aqueous solution behavior of $Ce^{IV}(PW_{11})_2$ was studied by means of ^{31}P and ^{31}P diffusion-ordered NMR spectroscopy (DOSY). The reactivity of $Ce^{IV}(PW_{11})_2$ was compared to two structurally analogous metal-substituted POMs, which contain Ce(III) and Eu(III) imbedded into the Keggin POM skeleton. To underpin the experimental findings and to elucidate the nature of the hydrolytically active species, the binding properties of NPP to $Ce^{IV}(PW_{11})_2$ and to its dissociation product $Ce^{IV}PW_{11}$ were theoretically investigated by means of density functional theory (DFT). In view of our previous reports (both on phosphodiester and peptide bond hydrolysis) where isopolyoxometalates or Zr-containing POMs were used as hydrolytic agents, this work demonstrates the first example of a phosphoesterase activity of a lanthanide-containing POM, namely, a Ce(IV)-containing Keggin-type POM, toward biological model systems. Unlike Zr(IV), Ce(IV) is prone to oxido/reduction chemistry, which opens the possibility to explore the effect of metal oxidation state on the hydrolytic activity by comparing activity of Ce(III) and Ce(IV) POMs, an approach that was not and could not be done with Zr(IV)-POMs. In addition to that, Zr(IV) and Ce(IV) have very different coordination chemistry, with Ce(IV) having potentially coordination number (CN) of 12, while Zr has typically CN = 8. We anticipated that this could have profound effect on the catalytic performance, as it can allow for multiple coordination of the substrate to the catalyst. This was confirmed by in-depth DFT calculations, which are not routinely done in polyoxometalate chemistry due to the large size and complexity of the metal cluster.

RESULTS AND DISCUSSION

Structure of Polyoxometalates and the Aqueous Solution Behavior of $(Ce^{IV}(PW_{11})_2$. The lanthanide-substituted Keggin POMs can adopt different structures. The 1:2 form ($Ln(PW_{11})_2$) in which the metal ion is sandwiched between two monolacunary α-Keggin POMs (Figure 1) has

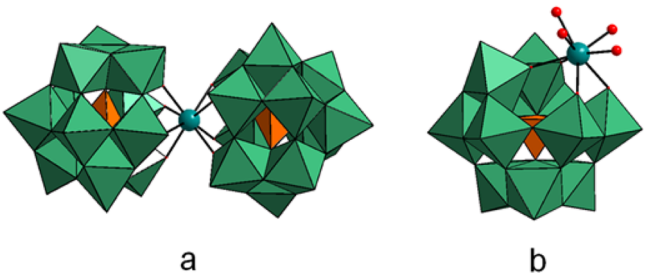

Figure 1. Structures of (a) the 1:2 dimeric lanthanide-substituted Keggin POMs $Ce^{III}(PW_{11})_2$, $Ce^{IV}(PW_{11})_2$, and $Eu^{III}(PW_{11})_2$[22,23] and (b) the Eu(III)-substituted 1:1 monomer Keggin POM.[23b] Ce(III)/Ce(IV)/Eu(III) are represented by green ball. The WO_6 groups are represented by sea-green octahedra, the internal PO_4 groups are represented by orange tetrahedra, and coordinated H_2O molecules are represented by red balls.

been proven by single-crystal X-ray diffraction for all three POMs under investigation in this study (Ln = Ce^{III}, Ce^{IV}, and Eu^{III}).[22] However, the 1:1 form ($LnPW_{11}$), composed of Ln cation coordinated to one monolacunary α-Keggin POM, has been fully characterized by X-ray crystallography only for Eu(III)-substituted POM ($EuPW_{11}$) shown in (Figure 1b).

The Ce(IV)-substituted Keggin-type POM was synthesized according to a procedure described in literature.[22a,23] Both NMR and X-ray analysis[22a] confirmed the 1:2 ($Ce^{IV}(PW_{11})_2$) nature of the POM. However, the existence of a 1:1 species $Ce^{IV}PW_{11}$, with structure analogous to $Eu^{III}PW_{11}$ shown in Figure 1b, has been also suggested in literature.[24] The previous work suggested that when $Ce^{IV}(PW_{11})_2$ is dissolved in D_2O, an equilibrium is formed between the 1:2 species (^{31}P chemical shift: −13.24 ppm)[25] and the 1:1 monomer (^{31}P chemical shift: −12.79 ppm)[24a] (Scheme 1). The distribution of these species is dependent on pD, concentration, temperature, and time.

DOI: 10.1021/acs.inorgchem.6b01802
Inorg. Chem. XXXX, XXX, XXX−XXX

Scheme 1. Equilibrium between the 1:2 and 1:1 Ce(IV)-Substituted Keggin-type Polyoxometalates

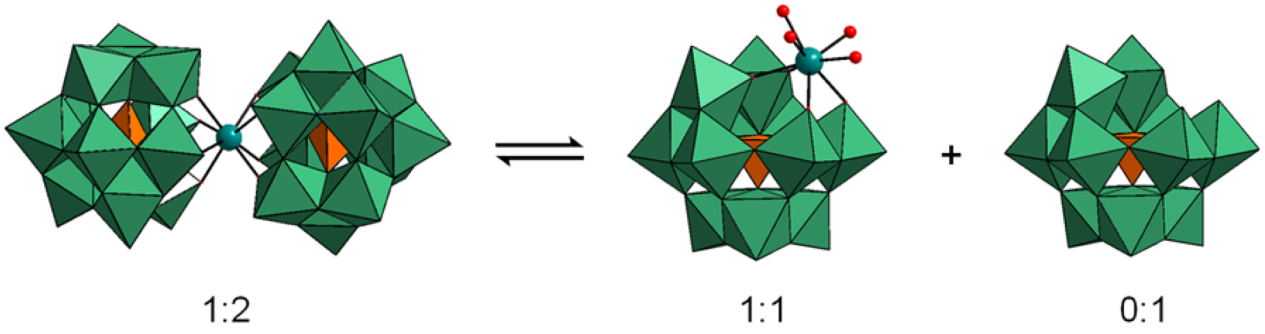

Since the maximal coordination number of Ce(IV) is 12,[26] the maximal free coordination sites available for complexation with the substrate of the 1:2 and 1:1 structure are most likely four and eight, respectively. However, in 1:2 species, the Ce(IV) center at which the substrate activation occurs is sterically hindered, because it is sandwiched between the two monolacunary Keggin ligands, while in the 1:1 species the Ce(IV) is more accessible for interaction with the substrate. Therefore, understanding the solution speciation of ($Ce^{IV}(PW_{11})_2$) under different conditions such as pH, concentration, temperature, and time is essential for understanding its catalytic activity. In addition, previous work with lanthanide[27] POMs has shown that oxidation state of the lanthanide ion has significant effect on the speciation and stability of the POM species.

To examine the effect of pD on the presence of the 1:1 and 1:2 types of structures of $Ce^{IV}(PW_{11})_2$ in aqueous solution, ^{31}P NMR spectra of 1.0 mM of $Ce^{IV}(PW_{11})_2$ in D_2O were recorded in the pD range from 0.9 to 10.4. As can be seen from Figure S1, only the 1:2 species (−13.24 ppm) was present from pD 3.4 to pD 10.4. Only at very low pH values (pD 0.9−2.4), the appearance of the 1:1 complex could be clearly detected at −12.79 ppm. In this range of pD the highest intensity of 1:1 complex was seen at pD 0.9. As can be seen from Scheme 1, an equivalent 0:1 species will be generated together with a 1:1 species. However, the expected signal of this monolacunary POM is not visible in some ^{31}P NMR spectra. This observation can be explained by the fact that this monolacunary species is possibly disintegrated to phosphate at ∼0 ppm and another spieces at −12.39 ppm. To increase the resolution of all signals, we measured ^{31}P NMR for 1.0 mM of $Ce^{IV}(PW_{11})_2$ in this range of pD without reference on 600 MHz (Figure S2). At pD 0.9 the signals of phosphate (∼0 ppm) and another spieces at −12.39 ppm are clearly seen.

The simultaneous existence of both $Ce^{IV}PW_{11}$ and $Ce^{IV}(PW_{11})_2$ at pD 0.9 was further supported by recording ^{31}P DOSY spectra of 6.0 mM $Ce^{IV}(PW_{11})_2$ solution after pD adjustment (Figure 2). Figure 2 shows that there are two species present with different diffusion coefficients. The faster-diffusing species (δ = −12.97 ppm)[24a] with a higher diffusion coefficient of 2.49 × 10^{-10} m^2 s^{-1} was assigned as $Ce^{IV}PW_{11}$, while the second species exhibiting NMR resonance at δ = −13.40 ppm and a diffusion coefficient of 1.99× 10^{-10} m^2 s^{-1} was assigned as $Ce^{IV}(PW_{11})_2$.

With the aim to compare the diffusion coefficients of $Ce^{IV}(PW_{11})_2$ at different pD values, ^{31}P DOSY NMR spectra of 6.0 mM $Ce^{IV}(PW_{11})_2$ at pD 6.4 and 8.4 were also recorded, and the results are shown in Figure S3 in the Supporting Information. From Figure S3 it can be seen that the diffusion coefficient of $Ce^{IV}(PW_{11})_2$ at these two pD values is the same and has a value of 1.80 × 10^{-10} m^2 s^{-1}, which is lower than that at pD 0.9. The ^1H DOSY spectra of water molecules in these samples (pD 0.9, 6.4, and 8.4) were also recorded, and the results showed that there was no change in the diffusion coefficients (14.5 × 10^{-10} m^2 s^{-1}) of the water molecules, suggesting that the viscosity of the samples under these conditions was the same. Therefore, the difference in the diffusion coefficients of $Ce^{IV}(PW_{11})_2$ at pD 0.9 in comparison with that at pD 6.4 and 8.4 may be explained by the fact that at very low pD value, $Ce^{IV}(PW_{11})_2$ is in equilibrium with a small amount of $Ce^{IV}PW_{11}$, resulting in its overall higher diffusion coefficient.

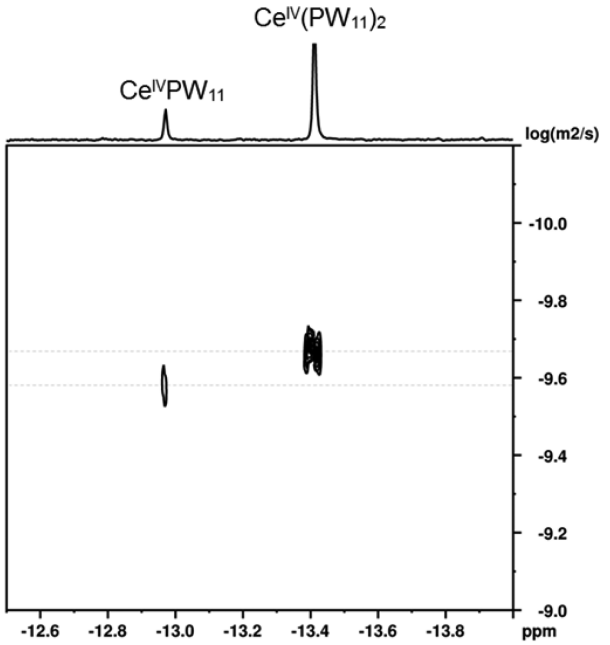

Figure 2. ^{31}P DOSY spectrum of 6.0 mM $Ce^{IV}(PW_{11})_2$ 1:2 at pD 0.9. The spectrum was recorded immediately after pD adjustment, no heating.

An additional experiment showed that at high pH values (pD 9.4) and 50 °C, after one week there was no conversion of $Ce^{IV}(PW_{11})_2$ into $Ce^{III}(PW_{11})_2$ POM; however, after two weeks 7.5% of $Ce^{IV}(PW_{11})_2$ was converted into $Ce^{III}(PW_{11})_2$ (δ = −17.91 ppm, 25% H_3PO_4),[22a,23] which is presumed to be hydrolytically less active, due to the weaker Lewis acidity of Ce(III) ion (Figure S4). At lower pD values (pD 6.4 and 8.4), there was no conversion from $Ce^{IV}(PW_{11})_2$ into $Ce^{III}(PW_{11})_2$ after two weeks at 50 °C, and therefore, pD of 6.4 was chosen for further studies.

DOI: 10.1021/acs.inorgchem.6b01802
Inorg. Chem. XXXX, XXX, XXX−XXX

Scheme 2. Hydrolysis of 4-Nitrophenylphosphate in the Presence of $Ce^{IV}(PW_{11})_2$

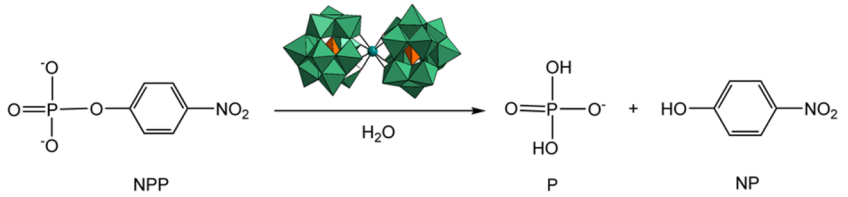

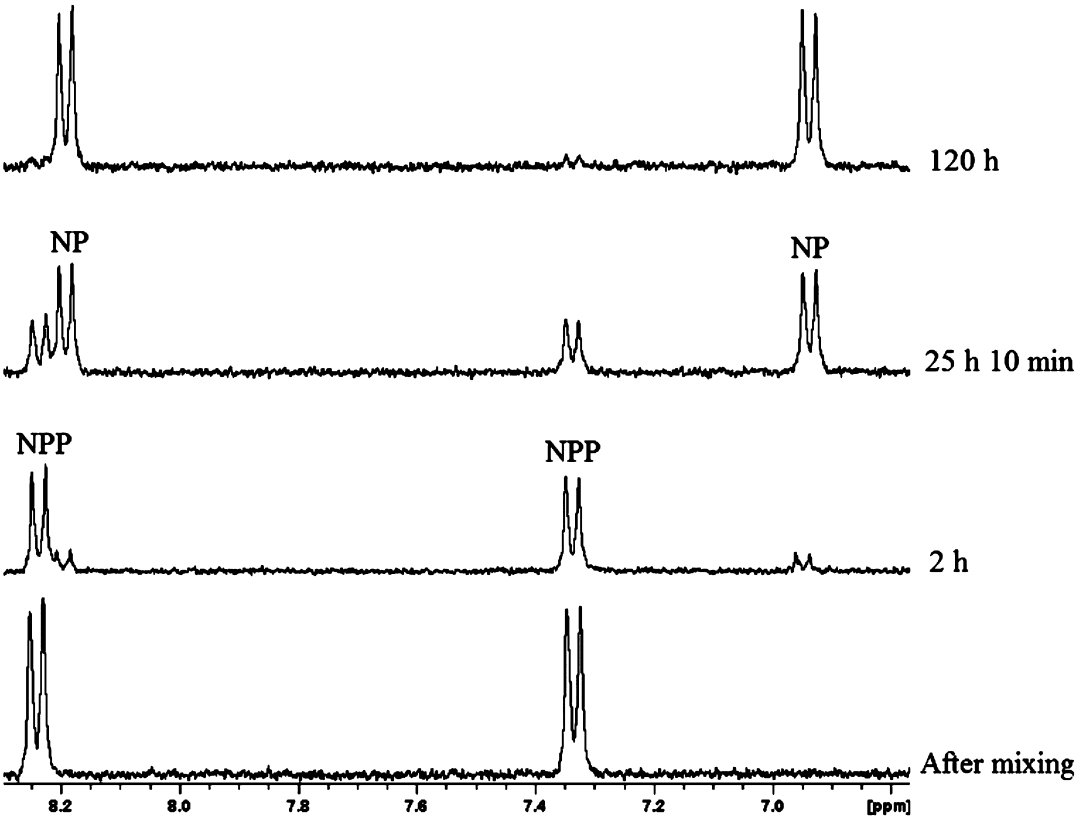

Figure 3. ^{1}H NMR of the hydrolysis reaction between 1.0 mM of NPP in the presence of 1.0 mM of $Ce^{IV}(PW_{11})_2$ at different time intervals at pD 6.4 and 50 °C.

By measuring ^{31}P NMR spectra of a $Ce^{IV}(PW_{11})_2$ solution with different concentrations (from 0.5 to 10.0 mM) at pD 6.4, the influence of concentration on speciation was investigated. Figure S5 shows that when the concentration of $Ce^{IV}(PW_{11})_2$ increases from 0.5 to 4.0 mM, only one peak at −13.24 ppm was observed. Therefore, it can be concluded that in this concentration range only the 1:2 species is present in solution. In the concentration range from 6.0 to 10.0 mM, besides a peak at −13.24 ppm, a very weak peak of monolacunary $[\alpha\text{-}PW_{11}O_{39}]^{7-}$ (δ −10.6 ppm)[28] was observed.

To evaluate the effect of temperature on the species distribution, a 1.0 mM sample at pD 6.4 was kept at a certain temperature for a week, and ^{31}P NMR spectra were recorded. From Figure S6, it can be seen that only the 1:2 species was present in solution when the temperature increased from 37 to 80 °C. This indicates that the 1:2 complex is stable within this temperature range. The effect of temperature on the species distribution was also examined at pD 0.9, where the intensity of the 1:1 complex is prominent. The spectra in Figure S7 show that when the temperature was increased from 37 to 80 °C, both 1:1 and 1:2 species are present in the sample. The prolonged incubation at high temperature promoted conversion of 1:2 into 1:1 species. After the species were mixed, the percentages of the 1:1 and 1:2 species were 38.5% and 61.5%, respectively; however, after 1 h at 80 °C both species were present in a 50:50 ratio (Table S1). The ionic strength did not have an influence on the speciation behavior of $Ce^{IV}(PW_{11})_2$, as the addition of up to 2.0 M concentration of LiCl did not result in any change in the ^{31}P NMR spectra.

The overall analysis of the data on speciation studies performed by ^{31}P NMR spectroscopy indicates that 1:2 is stable under a wide range of pH, concentration, and temperature conditions, while at pD values below 3.4 there is an equilibrium between the 1:2 and 1:1 species.

Hydrolysis of 4-Nitrophenylphosphate by Lanthanide-Substituted Polyoxometalates. The hydrolysis of NPP in the presence of $Ce^{IV}(PW_{11})_2$ (Scheme 2) was studied by means of ^{1}H NMR spectroscopy. An overview of the ^{1}H NMR spectra of NPP hydrolysis in the presence of $Ce^{IV}(PW_{11})_2$ at different reaction times is shown in Figure 3.

The hydrolysis of the P−O bond can be easily followed by the disappearance of the aromatic resonances of NPP at 8.24 and 7.33 ppm and the appearance of the aromatic NP resonances at 8.19 and 6.96 ppm. The signal of $H_2PO_4^-$

DOI: 10.1021/acs.inorgchem.6b01802
Inorg. Chem. XXXX, XXX, XXX−XXX

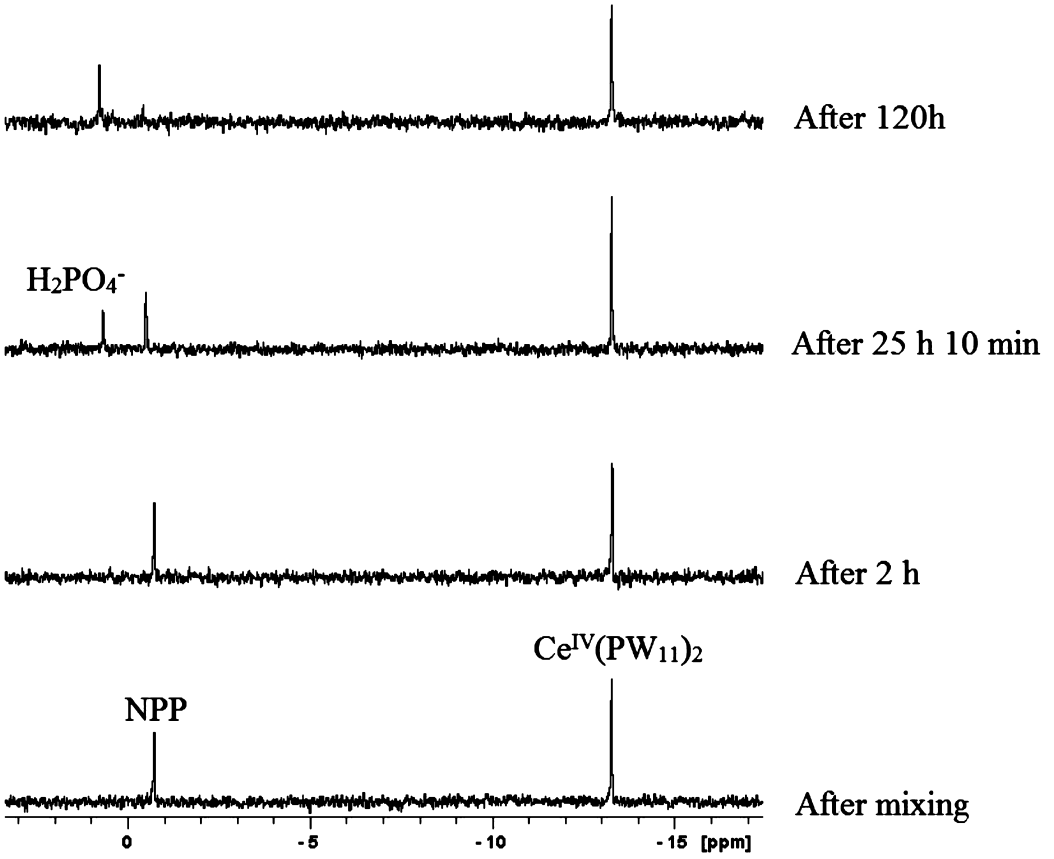

Figure 4. ^{31}P NMR of the hydrolysis reaction between 1.0 mM of NPP in the presence of 1.0 mM of $Ce^{IV}(PW_{11})_2$ at different time intervals at pD 6.4 and 50 °C.

f4

appears in ^{31}P spectra after 2 h (Figure 4), suggesting that the hydrolysis of P−O bond of NPP occurs.

To obtain the observed rate constant (k_{obs}) and half-life, the percentage of NPP at different time increments (Table S2) was calculated based on its ^{1}H NMR integration values. The percentages of NPP and NP as a function of reaction time are shown (Figure S8), and the natural logarithm of the concentration of NPP as a function of time (Figure S9) was fitted to a first-order linear decay function. At pD 6.4 and 50 °C in the presence of 1.0 mM $Ce^{IV}(PW_{11})_2$ an observed rate constant of $(5.31 \pm 0.06) \times 10^{-6}$ s^{-1} was calculated, representing nearly an order of magnitude acceleration as compared to the rate of spontaneous NPP hydrolysis. Hydrolysis of 1.0 mM of NPP was also followed in the presence of 1.0 mM of $Ce^{III}(PW_{11})_2$ (Figure S10) and 1.0 mM of $EuPW_{11}$ (Figure S11) by applying the same method, and the obtained rate constants had values k_{obs} $(1.12 \pm 0.06) \times 10^{-6}$ s^{-1} and $(1.07 \pm 0.06) \times 10^{-6}$ s^{-1}, respectively. Both $Ce^{III}(PW_{11})_2$ and $EuPW_{11}$ exhibited low reactivity toward NPP hydrolysis, which is not unusual considering their lower Lewis acid strength compared to Ce(IV), which has smaller radius and higher positive charge.[11a] The reaction between the Ce(IV) salt $(NH_4)_4Ce(SO_4)_4{\cdot}4H_2O$ and NPP was also examined in control experiments at pD 6.4 and 50 °C. In the presence of this Ce(IV) salt, the formation of insoluble gels[29] was observed, making a detailed kinetics analysis impossible. Under the same conditions, the reaction between NPP and the monolacunary Keggin POM ($[\alpha\text{-}PW_{11}O_{39}]^{7-}$) as well as trilacunary Keggin POM ($[A\text{-}\alpha\text{-}PW_9O_{34}]^{9-}$) did not result in observable NPP cleavage, suggesting that the presence of Ce(IV) was essential for the catalytic activity of the POM.

The hydrolysis of 1.0 mM BNPP in the presence of 1.0 mM $Ce^{IV}(PW_{11})_2$ was also observed under the same reaction conditions (pD 6.4 and 50 °C). However, this reaction is very slow to follow (30% of BNPP was hydrolyzed after nine weeks). Previous study showed that in the presence of 1.0 mM of $(Et_2NH_2)_8[\{\alpha\text{-}PW_{11}O_{39}Zr(\mu\text{-}OH)(H_2O)\}_2]{\cdot}7H_2O$ (ZrK 2:2), 1.0 mM BNPP hydrolysis at pD 6.4 and 60 °C proceeded with 320-fold rate enhancement in comparison to the spontaneous hydrolysis of BNPP.[8b] This rate enhancement is much higher than that of NPP hydrolysis in the presence of $Ce^{IV}(PW_{11})_2$ in the current study. The comparison of the hydrolytic activity of two these POMs is indirect, since different substrates were used. However, from these results $Ce^{IV}(PW_{11})_2$ was proposed to be less active than ZrK 2:2. The lower hydrolytic activity of $Ce^{IV}(PW_{11})_2$ in comparison to ZrK 2:2 can be explained by either DFT calculation or Lewis acid strength of metal center of POMs. DFT calculations demonstrated that ZrK 2:2→2 ZrK 1:1 is endergonic by 3.4 kcal mol^{-1}, and ZrK 1:1 is responsible for BNPP hydrolysis.[8c] In contrast, the splitting of $Ce^{IV}(PW_{11})_2$ into active species $Ce^{IV}PW_{11}$ needed more energy (28 kcal mol^{-1}) as shown below in the DFT calculation part. The lower hydrolytic activity of $Ce^{IV}PW_{11}$ in comparison to ZrK 1:1 can be explained by expected lower Lewis acid strength of Ce(IV) than Zr(IV), since both metal ions have the same charge, but the radius of Zr(IV) (0.84 Å)[30] is smaller than that of Ce(IV) (0.97 Å).[30]

Kinetics and Thermodynamic Parameters for the 4-Nitrophenylphosphate Hydrolysis by $Ce^{IV}(PW_{11})_2$. Since

DOI: 10.1021/acs.inorgchem.6b01802
Inorg. Chem. XXXX, XXX, XXX−XXX

pD plays an important role in the formation of different protonation states of NPP and its coordination to the POM, the effect of pD on the hydrolysis rate of NPP in the presence of $Ce^{IV}(PW_{11})_2$ was examined in the pD range from 3.4 to 9.4 (Figure 5 and Table S3). The rates for the spontaneous hydrolysis of NPP were also measured in this pH range, and the rate constants reported in Figure 5 were corrected for these values.

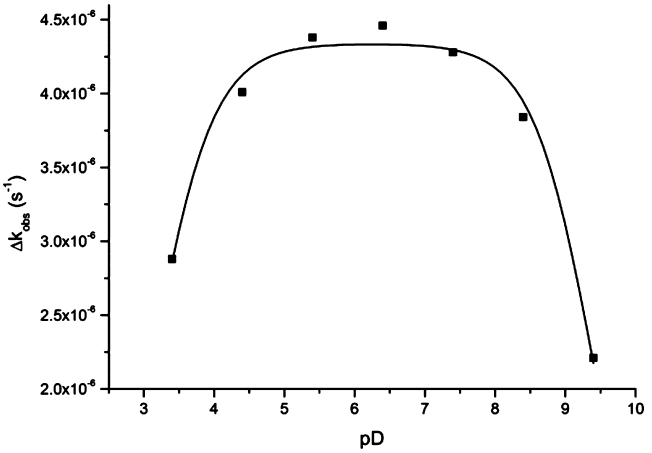

Figure 5. pD dependence of Δk_{obs} (the difference in k_{obs} for the hydrolysis of 1.0 mM of NPP in the presence and in the absence of 1.0 mM of $Ce^{IV}(PW_{11})_2$ at 50 °C).

The pD dependence of Δk_{obs} exhibits a bell-shaped profile, with fastest cleavage observed at pD 6.4. The data points were fitted to a Michaelis function (Equation 1), describing a bell-shaped dependence of the rate constant on pD.[31]

$$k_{obs} = k/(1 + h/K_1 + K_2/h) \quad (1)$$

In this equation, k_{obs} is the measured kinetic rate constant, k is the pH-independent turnover number, and $(1 + h/K_1 + K_2/h)$ is known as the Michaelis pH function in which $h = 1 \times 10^{-pD}$ represents the hydrogen-ion activity, while K_1 and K_2 are ionization constants associated with the enzyme, substrate(s), or other species in the reaction mixture.[32] The values of $k = 4.34 \times 10^{-6}$ s^{-1}, $pK_1 = 3.11$, and $pK_2 = 9.4$ were obtained by fitting the data points to Equation 1. The pK_1 value likely originates from the pK_a of NPP, which decreases upon metal binding.[32] Since the pK_a value of the water molecule that is bound to Ce(IV) is 1.1,[19a] this pK_a cannot contribute to pK_2 from the pD profile. The pK_2 value is most likely related to the pK_a of the phosphate,[33] which is one of the reaction products, that can also coordinate to Ce(IV) ion.

The speciation studies have shown that in the range of pD values from 3.4 to 9.4, $Ce^{IV}(PW_{11})_2$ exists as a 1:2 species, and therefore the observed pH dependence is due to the changes in the protonation state of NPP[34] and the intrinsic mechanism of metal-promoted phosphoester hydrolysis. Having a pK_a of 5.2,[35] in the acidic solutions NPP is protonated and exists mostly as a monoanion ($C_6H_5NO_6P^-$). The low pH therefore hinders effective coordination of NPP to Ce(IV) on the one hand, and on the other hand it results in protonation of water molecules, lowering their nucleophilic character. The mildly alkaline solutions are favorable for both the effective coordination of the substrate to Ce(IV) and the deprotonation of water molecules, which are the effective nucleophile in the hydrolytic reaction. The drop of Δk_{obs} in highly alkaline solutions is most likely due to the formation of hydrolytically inactive species and has been previously observed.[8b] In addition, in highly alkaline conditions, partial conversion of $Ce^{IV}(PW_{11})_2$ into kinetically inactive $Ce^{III}(PW_{11})_2$ can also occur (vide supra), which also results in slower NPP hydrolysis.

To investigate the binding between the substrate and $Ce^{IV}(PW_{11})_2$, the hydrolysis rate constant was determined for reaction mixtures containing 1.0 mM of NPP and increasing amounts of $Ce^{IV}(PW_{11})_2$ at pD 6.4. The values are listed in Table S4 and the general catalytic scheme for the hydrolysis of NPP in the presence of $Ce^{IV}(PW_{11})_2$ is shown in Scheme 3.

Scheme 3. General Catalytic Scheme for 4-Nitrophenylphosphate Hydrolysis by $Ce^{IV}(PW_{11})_2$

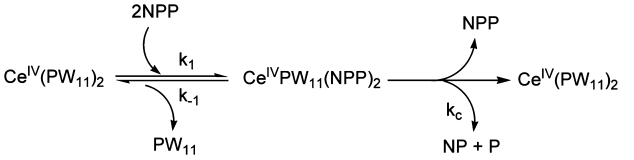

Scheme 3 was proposed based on the DFT calculation results that will be described in the following section. Although the DFT results suggest that the most stable complex involves two NPP ligands coordinated to Ce^{IV} in a monodentate fashion, it is unlikely that the hydrolysis of two NPP molecules occurs simultaneously. Therefore, one NPP molecule is proposed to be hydrolyzed at the time, and the rate-limiting step is most likely the hydrolysis of phosphoester bond, described with k_c in Scheme 3. More details are given in section Proposed Mechanism for the Hydrolysis of 4-Nitrophenylphosphate. By plotting the rate constants as a function of the concentration of $Ce^{IV}(PW_{11})_2$ (Figure 6) and fitting the data to Equation 2, the

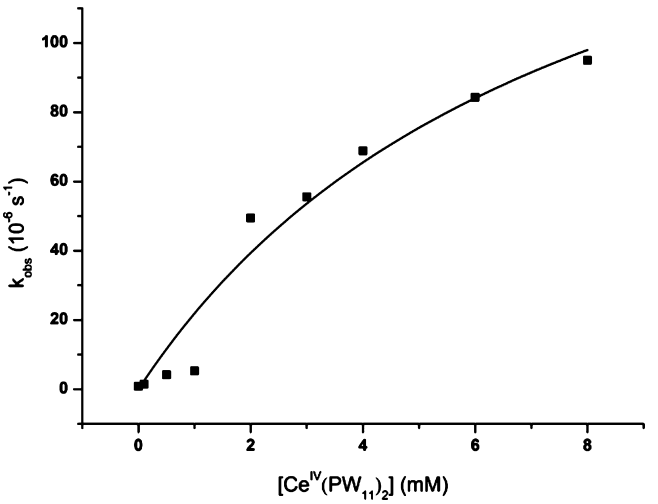

Figure 6. Influence of the concentration of $Ce^{IV}(PW_{11})_2$ on the observed rate constant for the hydrolysis of 1.0 mM of NPP at pD 6.4 and 50 °C.

binding constant ($K_f = k_1/k_{-1} = 127$ M^{-1}) and the catalytic rate constant ($k_c = 19.43 \times 10^{-5}$ s^{-1}) were obtained.

$$k_{obs} = \frac{k_c[Ce^{IV}PW_{11}]_0}{k_{-1}/k_1 + [Ce^{IV}PW_{11}]_0} \quad (2)$$

where $[Ce^{IV}PW_{11}]_0$ is the concentration of $Ce^{IV}PW_{11}$.

DOI: 10.1021/acs.inorgchem.6b01802
Inorg. Chem. XXXX, XXX, XXX−XXX

The data shown in Figure 6 indicate that 1 equiv of the POM can hydrolyze an excess of NPP. When 1.0 mM NPP and 0.1 mM of $Ce^{IV}(PW_{11})_2$ was used, the completion of NPP hydrolysis was still observed. This observation suggests that 1 equiv of $Ce^{IV}(PW_{11})_2$ hydrolyzes at least 10 equiv of NPP, demonstrating the catalytic function of the $Ce^{IV}(PW_{11})_2$. The recyclability of $Ce^{IV}(PW_{11})_2$ was examined by adding an extra amount (1.0 mM) of NPP to a fully hydrolyzed mixture of 1.0 mM NPP and 1.0 mM $Ce^{IV}(PW_{11})_2$ and adjusting the pD value of the reaction mixture to 6.4. The catalyst proved to be active after each cycle, and only slight decrease in the catalytic activity of 17% (Table S5) could be observed after the third cycle. The ^{31}P NMR spectra recorded after each completed reaction did not show any new signals as well as no change in the chemical shift of $Ce^{IV}(PW_{11})_2$, demonstrating the stability of $Ce^{IV}(PW_{11})_2$ in solution. Assuming that the decrease in the catalytic activity of $Ce^{IV}(PW_{11})_2$ is a linear fit as a function of reaction time, $Ce^{IV}(PW_{11})_2$ can be reused nearly 20 times.

As $Ce^{IV}(PW_{11})_2$ and NPP are both negatively charged species, the addition of salt to reaction mixture can affect the reaction rate. The influence of ionic strength on the reaction rate constant for NPP phosphoester bond hydrolysis was determined by adding LiCl to a mixture containing 1.0 mM of NPP and 1.0 mM of $Ce^{IV}(PW_{11})_2$. While LiCl did not influence the POM species distribution (vide supra) an increase of the rate constant was observed when the amount of LiCl was increased (Figure S12). Since the interaction between NPP and $Ce^{IV}(PW_{11})_2$ involves the repulsion between two negatively charged species ($C_6H_5NO_6P^-$ or $C_6H_4NO_6P^{2-}$ and $[Ce^{IV}(PW_{11}O_{39})_2]^{10-}$), the presence of salt plays an important role in shielding the charges of both negatively charged species and in diminishing the electrostatic repulsion between them.

The effect of temperature on the hydrolysis reaction rate was examined on a solution containing equimolar amounts of NPP and $Ce^{IV}(PW_{11})_2$ (1.0 mM) at pD 6.4 in the temperature range from 37 to 80 °C (Table S6). At higher temperatures increased reaction rates have been observed. The activation energy was calculated by the Arrhenius Equation 3.

$$\ln k_{obs} = \ln A - \frac{E_a}{R}\frac{1}{T} \quad (3)$$

In this equation, E_a represents the activation energy, R is the gas constant, and T is the temperature. Linear fitting of $\ln(k_{obs})$ as a function of $1/T$ (Figure S13a) results in an experimental activation energy (E_a) of 73.98 ± 1.05 kJ/mol.

The effect of temperature on a 1.0 mM of blank NPP solution at the same pD value in the temperature range from 50 to 80 °C was also followed and calculated using the similar method, resulting in an experimental activation energy (E_a) of 135.97 ± 1.87 kJ/mol. Obviously, in the presence of $Ce^{IV}(PW_{11})_2$, the activation energy of NPP hydrolysis significantly decreases.

The Eyring Equation 4 gives information on the activation enthalpy ($\Delta H^{\ddagger}$) and entropy ($\Delta S^{\ddagger}$) of the hydrolysis reaction.

$$\ln \frac{k_{obs}}{T} = \frac{-\Delta H^{\ddagger}}{R}\frac{1}{T} + \ln \frac{k_b}{h} + \frac{-\Delta S^{\ddagger}}{R} \quad (4)$$

In this equation, R represents the gas constant, $k_b = 1.38 \times 10^{-23}$ J/K is the Boltzmann constant, and $h = 6.626 \times 10^{-34}$ J/s is the Planck constant. Linear fitting of $\ln(k_{obs}/T)$ as a function of $1/T$ (Figure S13b) allows the calculation of the enthalpy of activation $\Delta H^{\ddagger}$ = 71.14 kJ/mol and the entropy of activation $\Delta S^{\ddagger}$ = −121.52 J/(mol K). The negative entropy of activation value is the result of the coordination of NPP to $Ce^{IV}(PW_{11})_2$. The Gibbs activation energy $\Delta G^{\ddagger}$ was calculated to be 110.39 kJ/mol at 50 °C. Despite the close correspondence in $\Delta H^{\ddagger}$ and $\Delta G^{\ddagger}$ compared to the values previously reported for phosphoester bond hydrolysis catalyzed by the Zr(IV)-substituted Wells−Dawson POM ($[Zr(\alpha_2\text{-}P_2W_{17}O_{61})_2]^{16-}$ ($\Delta G^{\ddagger}$ = 97.89 kJ mol^{-1}, $\Delta H^{\ddagger}$ = 74.54 kJ mol^{-1})[8a] a more negative $\Delta G^{\ddagger}$ value was observed for $Ce^{IV}(PW_{11})_2$. The much larger negative $\Delta S^{\ddagger}$ value could be due to the combination of many factors, including the lower negative charge of $[Ce^{IV}(PW_{11}O_{39})_2]^{10-}$ in comparison to that of $[Zr(\alpha_2\text{-}P_2W_{17}O_{61})_2]^{16-}$, larger radius of Ce(IV) (0.97 Å)[30] in comparison to that of Zr(IV) (0.84 Å),[30] and higher available coordination number of Ce(IV) (up to 12) in comparison to that of Zr(IV) (7).[36] These factors could facilitate binding of $Ce^{IV}(PW_{11})_2$ with the NPP substrate, leading to a more stable $[NPP\cdots Ce^{IV}(PW_{11})_2]$ transition state. However, the activation entropy is known as a parameter that is influenced by many factors such as change in solvation, molecularity, and conformation that cannot be rationalized or predicted. Therefore, it is difficult to conclude that the changes in activation entropy indicate changes in the reaction mechanism or changes in the binding of the phosphoester to metal complexes.[14a,37]

Investigation of the 4-Nitrophenylphosphate Binding to $Ce^{IV}(PW_{11})_2$ by Means of ^{31}P Nuclear Magnetic Resonance and Density Functional Theory Calculations. The interaction between NPP and $Ce^{IV}(PW_{11})_2$ was studied by ^{31}P NMR at pD 3.4 and 6.4. At pD 3.4 (Figure S14), a solution containing 2.0 mM of NPP displays a ^{31}P resonance signal at −4.67 ppm (half-width 5.28 Hz), while a solution containing 2.0 mM of $Ce^{IV}(PW_{11})_2$ is characterized by a peak at −13.24 ppm. When a ^{31}P spectrum of a mixture of 2.0 mM of NPP and 2.0 mM of $Ce^{IV}(PW_{11})_2$ at pD 3.4 was recorded, two signals were observed at −13.24 and −4.70 ppm (half-width 9.12 Hz). The peak of NPP was slightly shifted by 0.03 ppm, and the half-width was broadened by 3.84 Hz (Figure S15). This phenomenon may result from the fast exchange between the free NPP and the bound NPP. Both the small change in chemical shift and the line-broadening indicate that interaction between NPP and $Ce^{IV}(PW_{11})_2$ takes place.^{31}P spectra of the reaction mixture with and without reference compound were measured after 1 d at 50 °C. The signal at −4.70 ppm disappeared, and a new peak at 0.15 ppm appeared. This peak can be assigned to free phosphate (P), the reaction product of the NPP hydrolysis (Scheme 2).

At pD 6.4, $Ce^{IV}(PW_{11})_2$ has a chemical shift at −13.29 ppm, while the peak of NPP was observed at −1.33 ppm. In the presence of 2.0 mM of $Ce^{IV}(PW_{11})_2$ the peak of NPP shifted by 0.31 ppm and did not experience line-broadening (Figure S16). This shift confirmed that there is an interaction between NPP and $Ce^{IV}(PW_{11})_2$.

To obtain additional insights into the substrate−catalyst interactions and to identify the nature of the hydrolytically active species different NPP-POM complexes were modeled, and their aqueous phase stabilities were estimated by means of DFT theory and continuum solvent models including integral equation formalism polarizable continuum model (IEFPCM) and conductor-like polarizable continuum model (CPCM). First, the ability of the Ce^{IV} ion of $[Ce^{IV}(PW_{11})_2]^{10-}$ to bind a phosphate oxygen of NPP, thereby activating the phosphate P atom toward nucleophilic attack, was checked assuming

DOI: 10.1021/acs.inorgchem.6b01802
Inorg. Chem. XXXX, XXX, XXX−XXX

monodentate and bidentate NPP coordination. The optimized structure of the monodentate complex $[Ce^{IV}(PW_{11})_2(NPP\text{-}\kappa O)]^{12-}$ is shown in Figure 7. As can be seen, monodentate

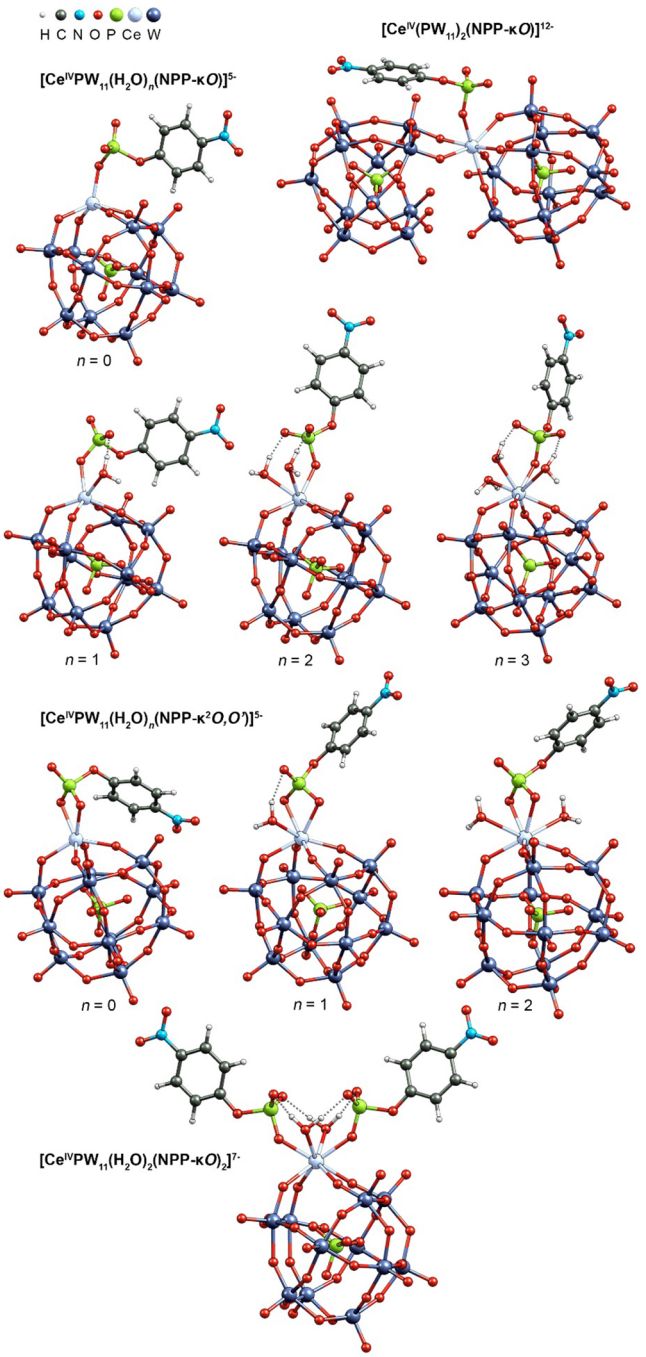

Figure 7. DFT-optimized complexes of $[Ce^{IV}(PW_{11})_2]^{10-}$ and $[Ce^{IV}PW_{11}]^{3-}$ with NPP.

coordination of NPP to Ce^{IV} causes partial displacement of one of the mono-lacunary Keggin ligands (two out of four oxygen donor atoms are detached from Ce^{IV}) thus reducing the coordination number of Ce^{IV} from eight in $[Ce^{IV}(PW_{11})_2]^{10-}$ to seven in the $[Ce^{IV}(PW_{11})_2(NPP\text{-}\kappa O)]^{12-}$ complex. The formation free energy calculated for this complex is 19 kcal mol^{-1} (see Table 1). Bidentate NPP coordination resulted in a similar complex (not shown in Figure 7) with a free energy of formation higher by 3.4 kcal mol^{-1} than for the monodentate

Table 1. Free Energy of Complex Formation[a] (kcal mol^{-1}) Calculated at the B3LYP/def2-TZVP Level of Theory with the IEFPCM and CPCM Solvation Models

NPP complex	IEFPCM	CPCM
$[Ce^{IV}(PW_{11})_2(NPP\text{-}\kappa O)]^{12-}$	18.6	18.9
$[Ce^{IV}PW_{11}(NPP\text{-}\kappa O)]^{5-}$	11.4	11.6
$[Ce^{IV}PW_{11}(H_2O)\ (NPP\text{-}\kappa O)]^{5-}$	0.9	1.2
$[Ce^{IV}PW_{11}(H_2O)_2(NPP\text{-}\kappa O)]^{5-}$	1.1	1.4
$[Ce^{IV}PW_{11}(H_2O)_3(NPP\text{-}\kappa O)]^{5-}$	−0.6	−0.2
$[Ce^{IV}PW_{11}(NPP\text{-}\kappa^2O,O')]^{5-}$	3.0	3.4
$[Ce^{IV}PW_{11}(H_2O)\ (NPP\text{-}\kappa^2O,O')]^{5-}$	5.8	6.1
$[Ce^{IV}PW_{11}(H_2O)_2(NPP\text{-}\kappa^2O,O')]^{5-}$	5.5	5.9
$[Ce^{IV}PW_{11}(H_2O)_2(NPP\text{-}\kappa O)_2]^{7-}$	−13.2	−13.1

[a]Calculated using the reactions $[Ce^{IV}(PW_{11})_2]^{10-} + NPP^{2-} \rightarrow [Ce^{IV}(PW_{11})_2(NPP\text{-}\kappa O)]^{12-}$ and $[Ce^{IV}(PW_{11})_2]^{10-} + nH_2O + mNPP^{2-} \rightarrow [Ce^{IV}PW_{11}(H_2O)_n(NPP)_m]^{(3+2m)-} + [PW_{11}]^{7-}$.

complex. Thus, according to the calculations binding of phosphate oxygen(s) of NPP to the Ce^{IV} ion of $[Ce^{IV}(PW_{11})_2]^{10-}$ is thermodynamically unlikely. Therefore, another explanation for the catalytic activity of the POM should be sought. As already suggested above, the $[Ce^{IV}PW_{11}]^{3-}$ species, which is a dissociation product of the parent POM, may possibly be responsible for the observed phosphoester hydrolysis. To check this hypothesis we estimated the free energy change associated with the reaction $[Ce^{IV}(PW_{11})_2]^{10-} + nH_2O \rightarrow [Ce^{IV}PW_{11}(H_2O)_n]^{3-} + [PW_{11}]^{7-}$, as well as the free energy of complexation between the resultant $[Ce^{IV}PW_{11}(H_2O)_n]^{3-}$ ion and NPP. In the above reaction the number of Ce^{IV}-bound water molecules (n) was varied from one to five to minimize the reaction energy. The lowest energy value (highest $[Ce^{IV}PW_{11}(H_2O)_n]^{3-}$ stabilization in solution) was found when four water ligands were bound to Ce^{IV}. The DFT-optimized $[Ce^{IV}PW_{11}(H_2O)_n]^{3-}$ structures and energy values can be found in Figure S17 and Table S7 of the Supporting Information. In the models with $n = 5$ one of the H_2O ligands detaches from Ce^{IV}during the optimization to form hydrogen bonds with a bridging Ce−O−W oxygen and the neighboring water ligands. Therefore, complexes with more than five water ligands have not been modeled. When using the energy of the $[Ce^{IV}PW_{11}(H_2O)_4]^{3-}$ species the calculated free energy of $[Ce^{IV}(PW_{11})_2]^{10-}$ splitting is rather high, 28 kcal mol^{-1}, (Table S7) which may explain the lack of ^{31}P NMR signals assigned to the $[Ce^{IV}PW_{11}]^{3-}$ product at near neutral pD. However, the addition of NPP might influence this equilibrium through formation of stable complexes with the monomeric species, thus compensating the energy loss associated with $[Ce^{IV}(PW_{11})_2]^{10-}$ splitting. Therefore, a variety of $[Ce^{IV}PW_{11}]^{3-}$ complexes involving NPP and H_2O ligands were modeled, and the net free energy change was estimated using the reaction

$$[Ce^{IV}(PW_{11})_2]^{10-} + nH_2O + mNPP^{2-} \rightarrow [Ce^{IV}PW_{11}(H_2O)_n(NPP)_m]^{(3+2m)-} + [PW_{11}]^{7-}$$

The NPP coordination mode and the number of ligands (both NPP and H_2O) were altered to find the most stable species. The optimized molecular structures of the different $[Ce^{IV}PW_{11}(H_2O)_n(NPP)_m]^{(3+2m)-}$ complexes are given in Figure 7, and the reaction free energies are collected in Table S7. In contrast to the parent POM, coordination of one NPP molecule to the monomeric species was found to be

DOI: 10.1021/acs.inorgchem.6b01802
Inorg. Chem. XXXX, XXX, XXX−XXX

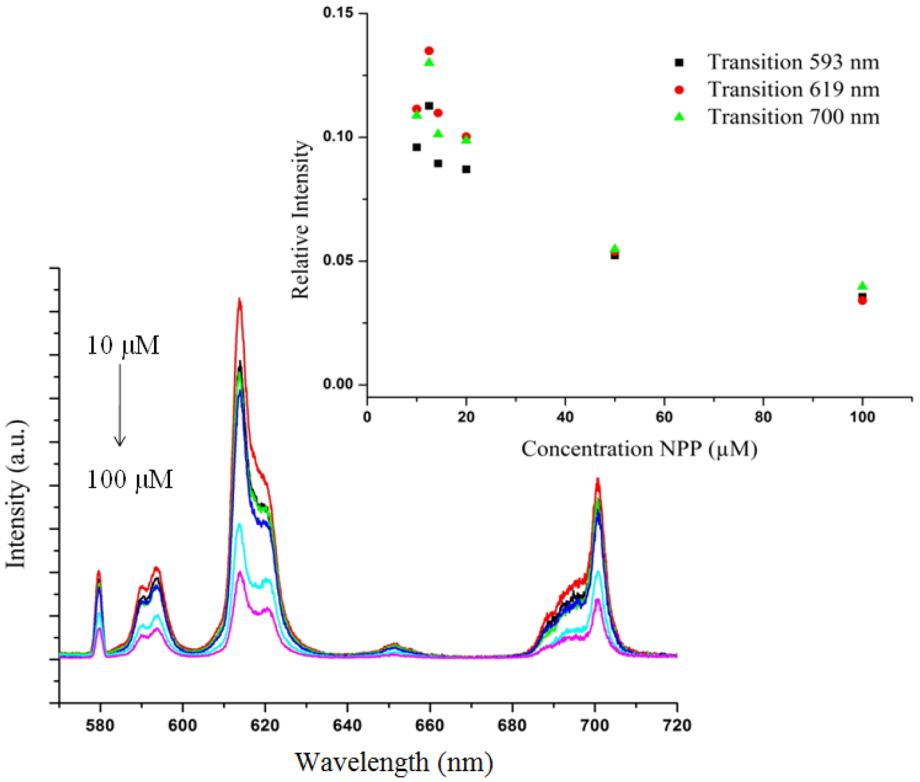

Figure 8. Steady-state emission spectra for the Eu(III)-substituted Keggin POM ($EuPW_{11}$; 100 μM) upon increasing concentration of NPP (10–100 μM) in aqueous solution at pD 6.4. (inset) The relative intensity decrease is depicted for the three main emission transitions: $^5D_0 \rightarrow {}^7F_1$ (593 nm, black ■), $^5D_0 \rightarrow {}^7F_2$ (619 nm, red ●), and $^5D_0 \rightarrow {}^7F_4$ (700 nm, green ▲).

thermodynamically favorable, with a free energy of complexation ranging from −16 to −28 kcal mol^{-1} (depending on the NPP/H_2O ratio and the NPP binding mode). With exception of $[Ce^{IV}PW_{11}(NPP\text{-}\kappa O)]^{5-}$ monodentate substrate binding is preferred over bidentate binding by 2–6 kcal mol^{-1}. Similar results were previously reported for the Zr^{IV} analogue of $[Ce^{IV}PW_{11}]^{3-}$.[8c] The most stable monodentate complex, $[Ce^{IV}PW_{11}(H_2O)_3(NPP\text{-}\kappa O)]^{5-}$, involves three H_2O ligands in addition to NPP, while in the bidentate complexes the addition of water ligands slightly decreases the computed stabilities. However, taking into account the free energy of $[Ce^{IV}(PW_{11})_2]^{10-}$ splitting, the formation of $[Ce^{IV}PW_{11}(H_2O)_3(NPP\text{-}\kappa O)]^{5-}$ species was calculated at the limit of reaction spontaneity ($\Delta G_{aq} \approx 0$ kcal mol^{-1}). To assess the energy change upon coordination of a second NPP ligand the lowest-energy monodentate complex was used for further modeling. The replacement of one Ce^{IV}-bound water in $[Ce^{IV}PW_{11}(H_2O)_3(NPP\text{-}\kappa O)]^{5-}$ by a NPP molecule resulted in a $[Ce^{IV}PW_{11}(H_2O)_2(NPP\text{-}\kappa O)_2]^{7-}$ complex, shown in Figure 7. The energy gain upon such substitution is estimated at ∼13 kcal mol^{-1}, lowering the net reaction free energy from 0 to −13 kcal mol^{-1}. Thus, the calculations predict that formation of $[Ce^{IV}PW_{11}]^{3-}$ complex(es) with two NPP ligands may take place in the reaction mixture.This in turn could explain the increased rate of phosphoester bond hydrolysis in the presence of POM as compared to the uncatalyzed reaction.

Investigation of the Interaction between 4-Nitrophenylphosphate and $EuPW_{11}$ by Luminescence Spectroscopy. Emission spectroscopy is an excellent tool to study coordination environment around Eu(III) in metal complexes. The structure of $EuPW_{11}$ is analogous to 1:1 Ce(IV); however, as $EuPW_{11}$ has been shown to be virtually inactive toward the hydrolysis of NPP, it can be used as a structural model to study the interaction between substrates and POMs by luminescence spectroscopy. The number of coordinated water molecules in $EuPW_{11}$ can be determined by measuring lifetimes of Eu(III) luminescence decay in H_2O and D_2O solutions.[38] The measurements performed on 100 μM concentration of $EuPW_{11}$ at pD 6.4 indicated presence of 4 water molecules in the first coordination sphere of Eu(III), consistent with its structure in the solid state.[23b]

Emission spectrum of $EuPW_{11}$ exhibits three main bands at 593, 619, and 700 nm, which can be attributed to $^5D_0 \rightarrow {}^7F_1$, $^5D_0 \rightarrow {}^7F_2$ and $^5D_0 \rightarrow {}^7F_4$ transitions, respectively. Gradual addition of NPP to $EuPW_{11}$ solution resulted in a significant decrease in the luminescence intensity of all three main transitions (Figure 8). These findings could indicate formation of $EuPW_{11}$/NPP complex, which is characterized with much lower emission intensity, resulting in the decrease of overall luminescence intensity. However, it is also plausible that the major excitation seems to occur at free NPP rather than at the POM/NPP complex, as $^5D_0 \rightarrow {}^7F_J$ transition does not exhibit significant change upon addition of $EuPW_{11}$. The NPP ligand shows a strong absorbance maximum at 310 nm, which is very close to the excitation wavelength of 291 nm; thus, most of the excitation light is likely to be absorbed by the ligand itself, leading to ineffective sensitization of Eu(III) ion in the $EuPW_{11}$/NPP complex. Unfortunately the photoluminescent experiments with $Eu(PW_{11})_2$/NPP system, which could help test this hypothesis, could not be performed, as our previous work has shown under low concentrations used in photoluminescent measurements the $Eu(PW_{11})_2$ fully dissociates into its monomeric $Eu(PW_{11})_2$ form.[39]

DOI: 10.1021/acs.inorgchem.6b01802
Inorg. Chem. XXXX, XXX, XXX–XXX

Scheme 4. Proposed Reaction Mechanism for the Hydrolysis of 4-Nitrophenylphosphate by $Ce^{IV}(PW_{11})_2$

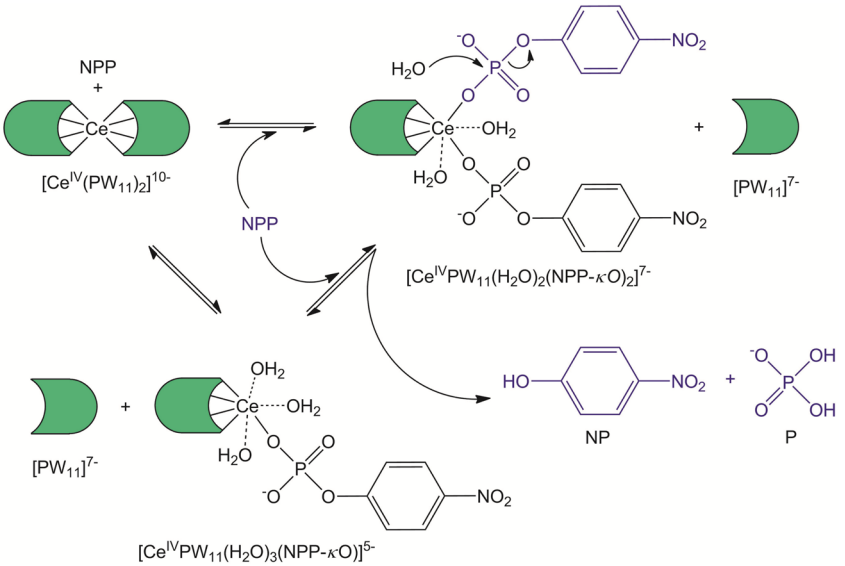

The formation of $EuPW_{11}$/NPP complex was however evidenced by ^{31}P NMR spectroscopy, which indicated that addition of excess of NPP to a solution of $EuPW_{11}$ resulted in the large shift ($\Delta\delta$ = 1.01 ppm) of ^{31}P NMR resonance in $EuPW_{11}$ (Figure S18). Although these experiments do indicate that interaction between NPP and the monomeric $EuPW_{11}$ occurs in solution, the low luminescence of the $EuPW_{11}$/NPP adduct prevents detailed analysis of the Eu(III) local environment in this complex.

Proposed Mechanism for the Hydrolysis of 4-Nitrophenylphosphate. Both Eu(III) luminescence and ^{31}P NMR spectroscopy data evidence the interaction between the NPP phosphate group and the lanthanide-substituted POMs in the reaction mixture. The Ce^{IV} ion in the parent catalyst $Ce^{IV}(PW_{11})_2$ is, however, hardly accessible by the substrate molecule, as it is sandwiched between the two bulky Keggin ligands. Theoretical calculations showed that the formation of an NPP complex with $Ce^{IV}(PW_{11})_2$ is thermodynamically unlikely. In contrast, the substrate molecule prefers to bind to the less sterically hindered monomeric species $Ce^{IV}PW_{11}$.The most stable complex involves two NPP ligands coordinated to Ce^{IV} in a monodentate fashion. Calculations show that the free energy gain associated with the formation of this complex is high enough to compensate for the free energy loss due to the splitting of $Ce^{IV}(PW_{11})_2$ to $Ce^{IV}PW_{11}$ and a monolacunary Keggin anion. On the basis of both experimental and theoretical findings a general model for the catalyzed hydrolysis of NPP is proposed; see Scheme 4. We consider the $[Ce^{IV}PW_{11}(H_2O)_2(NPP\text{-}\kappa O)_2]^{7-}$ complex to be the most probable hydrolytically active species. Coordination of an NPP phosphate oxygen atom to the Ce^{IV}center of $Ce^{IV}PW_{11}$ is expected to increase the positive charge at the phosphate P atom[8c] thus enhancing its susceptibility toward nucleophilic attack.[40]A previous study on $Zr^{IV}PW_{11}$ has shown that coordination of NPP^{2-} to Zr^{IV} dramatically increases the pK_a value of the Zr^{IV}-bound water molecule.[8c] Therefore, the presence of a Ce^{IV}–OH nucleophile and consequent intramolecular OH attack on the phosphate P atom are not expected. Moreover, phosphoester bond hydrolysis catalyzed by Ce^{IV} complexes involving Ce^{IV}–OH group(s) is much faster (by ~3 orders of magnitude) than the hydrolysis rate observed here.[41] Because metal-bound water molecules are weaker nucleophiles than uncoordinated water the actual nucleophilic attack on the P atom most likely involves a solvent water molecule by analogy with the uncatalyzed hydrolysis of NPP.[42] Since alteration of the reaction mechanism upon metal ion catalysis appears to be a general phenomenon, the mechanism of POM-promoted hydrolysis is most likely different from that of the uncatalyzed reaction. However, the main catalytic effect of the POM may be attributed to the Ce^{IV}-induced polarization of the substrate P–O bond in the $[Ce^{IV}PW_{11}(H_2O)_2(NPP\text{-}\kappa O)_2]^{7-}$ complex. Although this species involves two substrate molecules only one NPP molecule can be hydrolyzed at a time. This hydrolytic step is expected to be the rate-limiting reaction step, since the energy requirement for P–O bond cleavage is significantly higher than that associated with the ligand-exchange reactions in Scheme 4. Fast ligand exchange rates, typical for Ce(IV),[19b] implicate small energy barriers. The presence of such exchange between the free NPP and the bound NPP has already been suggested above based on the ^{31}P NMR spectra.

Hydrolysis of one of the NPP ligands in the active complex with liberation of the products, a phosphate anion and NP, may result in a less stable $[Ce^{IV}PW_{11}(H_2O)_n(NPP\text{-}\kappa O)]^{5-}$ species with one NPP ligand (Table 1), for example, $[Ce^{IV}PW_{11}(H_2O)_3(NPP\text{-}\kappa O)]^{5-}$, which in turn would favor the regeneration of the parent catalyst, $Ce^{IV}(PW_{11})_2$. Alternatively, another substrate molecule could bind to $[Ce^{IV}PW_{11}(H_2O)_3(NPP\text{-}\kappa O)]^{5-}$ to recover the hydrolytically active complex $[Ce^{IV}PW_{11}(H_2O)_2(NPP\text{-}\kappa O)_2]^{7-}$, where one of the NPP molecules is again hydrolyzed (as shown in Scheme 4). To further clarify the molecular mechanism of hydrolysis, additional investigations should be performed.

CONCLUSION

In this article, we report the detailed aqueous speciation study of $Ce^{IV}(PW_{11})_2$ POM under wide range of pD, initial POM concentration, temperature, and ionic strength. ^{31}P DOSY NMR studies showed that at very low pD, $Ce^{IV}(PW_{11})_2$ partially converts into the monomeric $Ce^{IV}PW_{11}$. Profound knowledge about aqueous distribution behavior of $Ce^{IV}(PW_{11})_2$ facilitated kinetics and thermodynamic studies of the hydrolysis

DOI: 10.1021/acs.inorgchem.6b01802
Inorg. Chem. XXXX, XXX, XXX–XXX

of NPP promoted by this POM. According to the DFT calculations coordination of a phosphate oxygen atom of NPP to the Ce^{IV} center of the parent catalyst $Ce^{IV}(PW_{11})_2$ is not likely. Instead, the substrate prefers to form complexes with the monomeric product $Ce^{IV}PW_{11}$, and in the most stable complex, which involves two NPP ligands coordinated to the Ce^{IV} center of $Ce^{IV}PW_{11}$ in a monodentate fashion, the formation energy exceeds the energy loss due to $Ce^{IV}(PW_{11})_2 \rightarrow Ce^{IV}PW_{11} + PW_{11}$ dissociation. Thus, it seems evident that the presence of NPP may provoke dissociation of the parent POM, which is otherwise thermodynamically unfavorable, to form a hydrolytically active complex with the monomer $[Ce^{IV}PW_{11}(H_2O)_2(NPP\text{-}\kappa O)_2]^{7-}$. Such dissociation of dimeric POM was recently confirmed for the Zr^{IV} analogue of $Ce^{IV}(PW_{11})_2$ in the presence of protein by means of single-crystal X-ray structural analysis.[43] The mechanism of hydrolysis most likely involves nucleophilic attack by a solvent water molecule on the activated P atom, instead of intramolecular attack by a Ce^{IV}–OH function. Our preliminary studies have shown that Zr^{IV}- and Ce^{IV}-substituted POMs are also active toward hydrolysis of plasmid DNA, demonstrating that negative charge of the POM does not impede its catalytic activity toward phosphodiester bonds.

EXPERIMENTAL SECTION

Materials. The lanthanide-substituted Keggin POMs, $[Me_2NH_2]_{11}[Ce^{III}(PW_{11}O_{39})_2]\cdot 14H_2O$[22a,23] ($Ce^{III}(PW_{11})_2$), $[Me_2NH_2]_{10}[Ce^{IV}(PW_{11}O_{39})_2]\cdot 14H_2O$[22a,23] ($Ce^{IV}(PW_{11})_2$), and $K_4[EuPW_{11}O_{39}]$[22b,23b] ($EuPW_{11}$) were prepared as described in the literature. Disodium 4-nitrophenylphosphate (NPP, $C_6H_4NO_6PNa_2\cdot 6H_2O$), DCl, and NaOD were purchased from Acros.

Kinetics Measurements. Solutions containing 1.0 mM of NPP and 1.0 mM of lanthanide-substituted POM were prepared in D_2O. The final pD of the solution was adjusted with minor amounts of 10% DCl and 15% NaOD solutions in D_2O. The pH-meter value was corrected by using the equation pD = pH meter reading +0.41.[44] The pD of the samples was measured at the beginning and at the end of hydrolysis, and the difference typically ranged from 0.5 to 1 unit due to the release of free phosphate as one of the reaction products of the cleavage reaction. The reaction mixture was kept at constant temperature, and ^1H NMR spectra were measured at certain time intervals during the hydrolytic reaction to calculate the observed rate constant (k_{obs}) by the integral method.

Nuclear Magnetic Resonance Spectroscopy. ^1H and ^{31}P NMR spectra were recorded on a Bruker Avance 400 spectrometer. As an internal standard 0.5 mM of 3-(trimethylsilyl)propionic-2,2,3,3-d_4 acid was present in the reaction solution. Phosphoric acid (25%) was used as a 0 ppm ^{31}P external reference. The DOSY spectra were measured on a Bruker Avance II+ 600 NMR spectrometer using 5 mm direct detection dual broad-band probe, with a gradient coil delivering maximum gradient strength of 53 G/cm. All experiments were performed at a temperature of 293 K. The ^{31}P DOSY spectra were acquired with the *Diff suite* integrated in the *Topspin 3.2* package by using the double-stimulated echo pulse sequence to compensate for possible convection during the experiments. The spectra were recorded with 32 000 time domain data points in t2 dimension, 32 gradient strength increments, diffusion delay (Δ) of 100 ms, gradient pulse length (δ) of 4 ms, relaxation delay of 3 s, and 64 transients for each gradient step. The gradient strength was varied from 2 to 70% of the maximum gradient output of the gradient unit (from 0.68 to 23.84 G/cm) to ensure complete signal attenuation. The spectra were processed with an exponential window function (line broadening factor 1), 32 000 data points in F2 dimension, and 512 data points in the diffusion dimension, using the fitting routine integrated in *Topspin 3.2* package. The evaluation of the diffusion coefficients was performed by fitting the diffusion profile (the normalized signal intensity as a function of the gradient strength G) at the chemical shift of each signal in the DOSY spectrum with an exponential function using the variant of Stejskal–Tanner equation adapted to the particular pulse sequence used.

Luminescence Spectroscopy Studies. Steady-state luminescence spectra were recorded on an Edinburgh Instruments FS900 steady-state spectrofluorimeter. Quartz cuvettes with 10.0 mm optical path length were used. Spectra were recorded with 100 μM $EuPW_{11}$ concentration in an unbuffered solution at pD 6.4 and at room temperature while monitoring the emission at 613 nm. Excitation of the sample took place at a wavelength of 291 nm unless stated otherwise. The emission slit widths were opened at 0.74 mm (resolution of 2.0 nm). The concentration of NPP increased stepwise from 0 to 100 μM.

Time-resolved luminescence spectra were recorded on an Edinburgh Instruments FS920 spectrofluorimeter. Quartz cuvettes with 10.0 mm optical path length were used. Spectra were recorded with 100 μM $EuPW_{11}$ concentration in an unbuffered solution at pD 6.4 and at room temperature. Excitation of the sample took place at a wavelength of 291 nm. The emission and excitation slit widths were opened at 0.74 mm (resolution of 2.0 nm).

Density Functional Theory Calculations. All calculations were performed with the Gaussian 09 Revision D.01 suite of programs[45] unless otherwise noted. Geometry optimizations and frequency calculations were performed with the B3LYP-D3[46] functional and 6-31G (d,p) basis sets. Cerium and tungsten atoms were described by means of MWB28[47] and LANL2DZ[48] effective core potentials (ECPs)/basis sets, respectively. The effects of the aqueous solvent were included in the geometry optimizations by means of the IEFPCM[49] continuum solvation model. To refine the electronic energies, single-point calculations were performed with the larger def2-TZVP basis sets.[50] The inner (core) electrons of W atoms were replaced with the MWB60[51] ECP, while for the Ce atom MWB28 ECP/basis set was still in use. For these calculations we used the B3LYP implementation in the ORCA program package,[52] version 3.0 and Grimme's atom-pairwise dispersion correction with Becke–Johnson damping (D3BJ).[46d,53] In addition to the IEFPCM model, solvation energies were also computed with the CPCM[54] solvation model, as in both cases the default UFF atomic radii were applied (at the level of theory used for geometry optimization). A standard state of 1 mol L^{-1} was used for all compounds except water molecules, for which 55.34 mol L^{-1} standard state was used instead.[55]

ASSOCIATED CONTENT

Supporting Information

^{31}P and ^{31}P DOSY NMR spectra, the percentage of $Ce^{IV}PW_{11}$ and $Ce^{IV}(PW_{11})_2$at pD 0.9 as a function of temperature, kinetics data, the recyclability data, DFT-optimized structures of the hydrated $[Ce^{IV}PW_{11}]^{3-}$ species and free energy of $[Ce^{IV}PW_{11}]^{3-}$ hydration. The Supporting Information is available free of charge on the ACS Publications website at DOI: 10.1021/acs.inorgchem.6b01802.

(PDF)

AUTHOR INFORMATION

Corresponding Author

*Phone: +32 16 327612. E-mail: tatjana.vogt@chem.kuleuven.be. Online: www.chem.kuleuven.be/lbc/.

Author Contributions

The manuscript was written through contributions of all authors. All authors have given approval to the final version of the manuscript.

Notes

The authors declare no competing financial interest.

DOI: 10.1021/acs.inorgchem.6b01802
Inorg. Chem. XXXX, XXX, XXX–XXX

■ ACKNOWLEDGMENTS

T.N.P.V. thanks KU Leuven for the financial support. T.K.N.L. thanks the Vietnamese Government and KU Leuven for a doctoral fellowship. G.A. thanks F. W. O. Flanders for a postdoctoral fellowship. T.T.M. thanks the F. W. O. Flanders for the financial support under Project No. G.0260.12. The computational resources and services used in this work were provided by the Flemish Supercomputer Center, funded by the Hercules Foundation and the Flemish Government−department EWI. The calculations were performed on the HPC cluster Tier-2 of KU Leuven.

■ REFERENCES

(1) (a) Proust, A.; Thouvenot, R.; Gouzerh, P. Functionalization of polyoxometalates: towards advanced applications in catalysis and materials science. *Chem. Commun.* **2008**, *16*, 1837−1852. (b) Long, D.-L.; Tsunashima, R.; Cronin, L. Polyoxometallate als Bausteine für funktionelle Nanosysteme. *Angew. Chem.* **2010**, *122* (10), 1780−1803. (c) Long, D.-L.; Tsunashima, R.; Cronin, L. Polyoxometalates: Building Blocks for Functional Nanoscale Systems. *Angew. Chem., Int. Ed.* **2010**, *49* (10), 1736−1758.

(2) Berzelius, J. J. Beitrag zur näheren Kenntniss des Molybdäns. *Ann. Phys.* **1826**, *82*, 369−392.

(3) (a) Errington, R. J.; Wingad, R. L.; Clegg, W.; Elsegood, M. R. J. Direct bromination of Keggin fragments to give $PW_9O_{28}Br_6^{3-}$: A polyoxotungstate with a hexabrominated face. *Angew. Chem., Int. Ed.* **2000**, *39* (21), 3884−3886. (b) Bereau, V.; Cadot, E.; Bogge, H.; Muller, A.; Secheresse, F. Addition of $\{M_2S_2O_2\}^{2+}$, M = Mo, W, to A-α-$[PW_9O_{34}]^{9-}$. Synthesis and structural characterizations in the solid state and in solution. *Inorg. Chem.* **1999**, *38* (25), 5803−5808. (c) Bino, A.; Ardon, M.; Lee, D.; Spingler, B.; Lippard, S. J. Synthesis and structure of $[Fe_{13}O_4F_{24}(OMe)_{12}]^{5-}$: The first open-shelf Keggin ion. *J. Am. Chem. Soc.* **2002**, *124* (17), 4578−4579.

(4) (a) Carraro, M.; Gross, S. Hybrid Materials Based on the Embedding of Organically Modified Transition Metal Oxoclusters or Polyoxometalates into Polymers for Functional Applications: A Review. *Materials* **2014**, *7* (5), 3956−3989. (b) Proust, A.; Matt, B.; Villanneau, R.; Guillemot, G.; Gouzerh, P.; Izzet, G. Functionalization and post-functionalization: a step towards polyoxometalate-based materials. *Chem. Soc. Rev.* **2012**, *41* (22), 7605−7622.

(5) (a) Clemente-Juan, J. M.; Coronado, E.; Gaita-Arino, A. Magnetic polyoxometalates: from molecular magnetism to molecular spintronics and quantum computing. *Chem. Soc. Rev.* **2012**, *41* (22), 7464−7478. (b) Seemann, K. M.; Bauer, A.; Kindervater, J.; Meyer, M.; Besson, C.; Luysberg, M.; Durkin, P.; Pyckhout-Hintzen, W.; Budisa, N.; Georgii, R.; Schneider, C. M.; Kogerler, P. Polyoxometalate-stabilized, water dispersible Fe_2Pt magnetic nanoparticles. *Nanoscale* **2013**, *5* (6), 2511−2519.

(6) (a) Stracke, J. J.; Finke, R. G. Electrocatalytic Water Oxidation Beginning with the Cobalt Polyoxometalate $[Co_4(H_2O)_2(PW_9O_{34})_2]^{10-}$: Identification of Heterogeneous CoO_x as the Dominant Catalyst. *J. Am. Chem. Soc.* **2011**, *133* (38), 14872−14875. (b) Izarova, N. V.; Pope, M. T.; Kortz, U. Noble Metals in Polyoxometalates. *Angew. Chem., Int. Ed.* **2012**, *51* (38), 9492−9510. (c) Sartorel, A.; Bonchio, M.; Campagna, S.; Scandola, F. Tetrametallic molecular catalysts for photochemical water oxidation. *Chem. Soc. Rev.* **2013**, *42* (6), 2262−2280.

(7) (a) Ogata, A.; Mitsui, S.; Yanagie, H.; Kasano, H.; Hisa, T.; Yamase, T.; Eriguchi, M. A novel anti-tumor agent, polyoxomolybdate induces apoptotic cell death in AsPC-1 human pancreatic cancer cells. *Biomed. Pharmacother.* **2005**, *59* (5), 240−244. (b) Yamase, T. Anti-tumor, -viral, and -bacterial activities of polyoxometalates for realizing an inorganic drug. *J. Mater. Chem.* **2005**, *15* (45), 4773−4782. (c) Hasenknopf, B.; Micoine, K.; Lacote, E.; Thorimbert, S.; Malacria, M.; Thouvenot, R. Chirality in Polyoxometalate Chemistry. *Eur. J. Inorg. Chem.* **2008**, *2008*, 5001−5013. (d) Wang, X. H.; Li, F.; Liu, S. X.; Pope, M. T. New liposome-encapsulated-polyoxometalates: synthesis and antitumoral activity. *J. Inorg. Biochem.* **2005**, *99* (2), 452−457. (e) Cindric, M.; Novak, T. K.; Kraljevic, S.; Kralj, M.; Kamenar, B. Structural and antitumor activity study of gamma-octamolybdates containing aminoacids and peptides. *Inorg. Chim. Acta* **2006**, *359* (5), 1673−1680. (f) Mitsui, S.; Ogata, A.; Yanagie, H.; Kasano, H.; Hisa, T.; Yamase, T.; Eriguchi, M. Antitumor activity of polyoxomolybdate, $[NH_3Pr^i]_6[Mo_7O_{24}]\cdot 3H_2O$, against, human gastric cancer model. *Biomed. Pharmacother.* **2006**, *60* (7), 353−358. (g) Stephan, H.; Kubeil, M.; Emmerling, F.; Müller, C. E. Polyoxometalates as Versatile Enzyme Inhibitors. *Eur. J. Inorg. Chem.* **2013**, *2013* (10−11), 1585−1594.

(8) (a) Vanhaecht, S.; Absillis, G.; Parac-Vogt, T. N. Hydrolysis of DNA model substrates catalyzed by metal-substituted Wells-Dawson polyoxometalates. *Dalton Trans.* **2012**, *41* (33), 10028−10034. (b) Luong, T. K. N.; Absillis, G.; Shestakova, P.; Parac-Vogt, T. N. Solution Speciation of the Dinuclear Zr^{IV}-Substituted Keggin Polyoxometalate $[\{\alpha\text{-}PW_{11}O_{39}Zr(\mu\text{-}OH)(H_2O)\}_2]^{8-}$ and Its Reactivity towards DNA-Model Phosphodiester Hydrolysis. *Eur. J. Inorg. Chem.* **2014**, *2014* (31), 5276−5284. (c) Luong, T. K. N.; Shestakova, P.; Mihaylov, T. T.; Absillis, G.; Pierloot, K.; Parac-Vogt, T. N. Multinuclear Diffusion NMR Spectroscopy and DFT Modeling: A Powerful Combination for Unraveling the Mechanism of Phosphoester Bond Hydrolysis Catalyzed by Metal-Substituted Polyoxometalates. *Chem. - Eur. J.* **2015**, *21* (11), 4428−4439. (d) Luong, T. K. N.; Absillis, G.; Shestakova, P.; Parac-Vogt, T. N. Hydrolysis of the RNA model substrate catalyzed by a binuclear Zr^{IV}-substituted Keggin polyoxometalate. *Dalton Trans.* **2015**, *44* (35), 15690−15696.

(9) (a) Absillis, G.; Parac-Vogt, T. N. Peptide Bond Hydrolysis Catalyzed by the Wells-Dawson $Zr(\alpha_2\text{-}P_2W_{17}O_{61})_2$ Polyoxometalate. *Inorg. Chem.* **2012**, *51* (18), 9902−9910. (b) Ly, H. G. T.; Absillis, G.; Parac-Vogt, T. N. Amide bond hydrolysis in peptides and cyclic peptides catalyzed by a dimeric Zr(IV)-substituted Keggin type polyoxometalate. *Dalton Trans.* **2013**, *42* (30), 10929−10938. (c) Ly, H. G. T.; Absillis, G.; Bajpe, S. R.; Martens, J. A.; Parac-Vogt, T. N. Hydrolysis of Dipeptides Catalyzed by a Zirconium(IV)-Substituted Lindqvist Type Polyoxometalate. *Eur. J. Inorg. Chem.* **2013**, *2013* (26), 4601−4611.

(10) (a) Boglio, C.; Lemière, G.; Hasenknopf, B.; Thorimbert, S.; Lacôte, E.; Malacria, M. Lanthanide Complexes of the Monovacant Dawson Polyoxotungstate $[\alpha_1\text{-}P_2W_{17}O_{61}]^{10-}$ as Selective and Recoverable Lewis Acid Catalysts. *Angew. Chem., Int. Ed.* **2006**, *45* (20), 3324−3327. (b) Xuan, W.-J.; Botuha, C.; Hasenknopf, B.; Thorimbert, S. Addition of carbon nucleophiles to hemiaminals promoted by a Lewis acidic polyoxotungstate. *Org. Chem. Front.* **2014**, *1* (9), 1091−1095. (c) Dupré, N.; Rémy, P.; Micoine, K.; Boglio, C.; Thorimbert, S.; Lacôte, E.; Hasenknopf, B.; Malacria, M. Chemoselective Catalysis with Organosoluble Lewis Acidic Polyoxotungstates. *Chem. - Eur. J.* **2010**, *16* (24), 7256−7264. (d) Suzuki, K.; Sugawa, M.; Kikukawa, Y.; Kamata, K.; Yamaguchi, K.; Mizuno, N. Strategic Design and Refinement of Lewis Acid−Base Catalysis by Rare-Earth-Metal-Containing Polyoxometalates. *Inorg. Chem.* **2012**, *51* (12), 6953−6961.

(11) (a) Hegg, E. L.; Burstyn, J. N. Toward the development of metal-based synthetic nucleases and peptidases: a rationale and progress report in applying the principles of coordination chemistry. *Coord. Chem. Rev.* **1998**, *173*, 133−165. (b) Komiyama, M.; Takeda, N.; Shigekawa, H. Hydrolysis of DNA and RNA by lanthanide ions: mechanistic studies leading to new applications. *Chem. Commun.* **1999**, *16*, 1443−1451. (c) Kramer, R. Bioinorganic models for the catalytic cooperation of metal ions and functional groups in nuclease and peptidase enzymes. *Coord. Chem. Rev.* **1999**, *182*, 243−261. (d) Blasko, A.; Bruice, T. C. Recent studies of nucleophilic, general-acid, and metal ion catalysis of phosphate diester hydrolysis. *Acc. Chem. Res.* **1999**, *32* (6), 475−484.

(12) Absillis, G.; Van Deun, R.; Parac-Vogt, T. N. Polyoxomolybdate Promoted Hydrolysis of a DNA-Model Phosphoester Studied by NMR and EXAFS Spectroscopy. *Inorg. Chem.* **2011**, *50* (22), 11552−11560.

DOI: 10.1021/acs.inorgchem.6b01802
Inorg. Chem. XXXX, XXX, XXX−XXX

(13) Rawlings, J.; Cleland, W. W.; Hengge, A. C. Metal-catalyzed phosphodiester cleavage: Secondary ^{18}O isotope effects as an indicator of mechanism. *J. Am. Chem. Soc.* **2006**, *128* (51), 17120−17125.
(14) (a) Fry, F. H.; Fischmann, A. J.; Belousoff, M. J.; Spiccia, L.; Brugger, J. Kinetics and Mechanism of Hydrolysis of a Model Phosphate Diester by $[Cu(Me_3tacn)(OH_2)_2]^{2+}$ (Me_3tacn = 1,4,7-Trimethyl-1,4,7-triazacyclononane). *Inorg. Chem.* **2005**, *44* (4), 941−950. (b) Hegg, E. L.; Mortimore, S. H.; Cheung, C. L.; Huyett, J. E.; Powell, D. R.; Burstyn, J. N. Structure-reactivity studies in copper(II)-catalyzed phosphodiester hydrolysis. *Inorg. Chem.* **1999**, *38* (12), 2961−2968.
(15) Gomez-Tagle, P.; Yatsimirsky, A. K. Phosphodiester hydrolysis by lanthanide complexes of bis-tris propane. *Inorg. Chem.* **2001**, *40* (15), 3786−3796.
(16) (a) Shangguan, G. Q.; Zhu, J.; Wang, N.; Ni, J. Z. Phosphate diester hydrolysis by dinuclear Tb(III) complexes with BDBPH in second-order dependence. *Chin. Chem. Lett.* **2006**, *17* (1), 89−92. (b) Aguilar-Perez, F.; Gomez-Tagle, P.; Collado-Fregoso, E.; Yatsimirsky, A. K. Phosphate ester hydrolysis by hydroxo complexes of trivalent lanthanides stabilized by 4-imidazolecarboxylate. *Inorg. Chem.* **2006**, *45* (23), 9502−9517.
(17) (a) Hurst, P.; Takasaki, B. K.; Chin, J. Rapid Cleavage of RNA with a La(III) Dimer. *J. Am. Chem. Soc.* **1996**, *118* (41), 9982−9983. (b) Baker, B. F.; Khalili, H.; Wei, N.; Morrow, J. R. Cleavage of the 5′ Cap Structure of mRNA by a Europium(III) Macrocyclic Complex with Pendant Alcohol Groups. *J. Am. Chem. Soc.* **1997**, *119* (38), 8749−8755. (c) Yashiro, M.; Ishikubo, A.; Komiyama, M. Dinuclear lanthanum(III) complex for efficient hydrolysis of RNA. *J. Biochem.* **1996**, *120* (6), 1067−1069.
(18) (a) Cowan, J. A. Chemical nucleases. *Curr. Opin. Chem. Biol.* **2001**, *5* (6), 634−642. (b) Franklin, S. J. Lanthanide-mediated DNA hydrolysis. *Curr. Opin. Chem. Biol.* **2001**, *5* (2), 201−208. (c) Chin, J. Artificial dinuclear phosphoesterases. *Curr. Opin. Chem. Biol.* **1997**, *1* (4), 514−521.
(19) (a) Komiyama, M.; Takeda, N.; Shigekawa, H. Hydrolysis of DNA and RNA by lanthanide ions: mechanistic studies leading to new applications. *Chem. Commun.* **1999**, *0* (16), 1443−1451. (b) Bonomi, R.; Scrimin, P.; Mancin, F. Phosphate diesters cleavage mediated by Ce(IV) complexes self-assembled on gold nanoparticles. *Org. Biomol. Chem.* **2010**, *8* (11), 2622−2626.
(20) Zhao, M.; Zhao, C.; Jiang, X. Q.; Ji, L. N.; Mao, Z.-W. Rapid hydrolysis of phosphate ester promoted by Ce(IV) conjugating with a β-cyclodextrin monomer and dimer. *Dalton Trans.* **2012**, *41*, 4469−4476.
(21) Stroobants, K.; Moelants, E.; Ly, H. G. T.; Proost, P.; Bartik, K.; Parac-Vogt, T. N. Polyoxometalates as a Novel Class of Artificial Proteases: Selective Hydrolysis of Lysozyme under Physiological pH and Temperature Promoted by a Cerium(IV) Keggin-Type Polyoxometalate. *Chem. - Eur. J.* **2013**, *19* (8), 2848−2858.
(22) (a) Iijima, J.; Ishikawa, E.; Nakamura, Y.; Naruke, H. Synthesis and structural investigation of sandwich polyoxotungstates containing cerium (III/IV) and mono-lacunary Keggin tungstophosphate units. *Inorg. Chim. Acta* **2010**, *363* (7), 1500−1506. (b) Huang, W. L.; Schopfer, M.; Zhang, C.; Howell, R. C.; Gee, B. A.; Francesconi, L. C.; Polenova, T. Probing local environments in paramagnetic Europium-substituted Keggin solids by ^{31}P magic angle spinning NMR spectroscopy. *J. Phys. Chem. B* **2006**, *110* (25), 12340−12350.
(23) (a) Ginsberg, A. P. In *Inorganic Syntheses;* John Wiley & Sons, 1990; Vol. *27*, p 100. (b) Zhang, C.; Howell, R. C.; Scotland, K. B.; Perez, F. G.; Todaro, L.; Francesconi, L. C. Aqueous speciation studies of europium(III) phosphotungstate. *Inorg. Chem.* **2004**, *43* (24), 7691−7701.
(24) (a) Maksimov, G. M.; Maksimovskaya, P. I.; Kozhevnikov, I. V. Heteropoly acids derived from the complexes of the $PW_{11}O_{39}^{7-}$ anion with metal cations. *Russ. J. Inorg. Chem.* **1992**, *37*, 2279−2286. (b) Bassil, B. S.; Kortz, U. Recent Advances in Lanthanide-Containing Polyoxotungstates. *Z. Anorg. Allg. Chem.* **2010**, *636* (12), 2222−2231. (c) Wang, K.-Y.; Bassil, B. S.; Lin, Z.; Römer, I.; Vanhaecht, S.; Parac-Vogt, T. N.; Sáenz de Pipaón, C.; Galán-Mascarós, J. R.; Fan, L.; Cao, J.; Kortz, U. Ln_{12}-Containing 60-Tungstogermanates: Synthesis, Structure, Luminescence, and Magnetic Studies. *Chem. - Eur. J.* **2015**, *21* (50), 18168−18176.
(25) Fedotov, M. A.; Maksimovskaya, R. I. NMR structural aspects of the chemistry of V, Mo, W polyoxometalates. *J. Struct. Chem.* **2006**, *47* (5), 952−978.
(26) Cotton, S. In *Lanthanide and Actinide Chemistry;* John Wiley & Sons, 2006; pp 55−57.
(27) Jing, J.; Burton-Pye, B. P.; Francesconi, L. C.; Antonio, M. R. Europium(III) Reduction and Speciation within a Wells−Dawson Heteropolytungstate. *Inorg. Chem.* **2008**, *47* (15), 6889−6899.
(28) (a) Maksimov, G. M.; Maksimovskaya, R. I. On the $P_2W_{16}O_{60}^{14-}$ heteropolyanion synthesis. *Polyhedron* **1996**, *15* (23), 4275−4276. (b) Sokolov, M. N.; Chubarova, E. V.; Peresypkina, E. V.; Virovets, A. V.; Fedin, V. P. S. Complexes of Zr^{IV} and Hf^{IV} with Monolacunary Keggin and Dawson-type Anions. *Russ. Chem. Bull.* **2007**, *56* (2).22010.1007/s11172-007-0036-x
(29) Zhao, M.; Zhao, C.; Jiang, X. Q.; Ji, L. N.; Mao, Z. W. Rapid hydrolysis of phosphate ester promoted by Ce(IV) conjugating with a β-cyclodextrin monomer and dimer. *Dalton Trans.* **2012**, *41*, 4469−4476.
(30) Thomas, J. B.; Bodnar, R. J.; Shimizu, N.; Chesner, C. A. Melt Inclusions in Zircon. *Rev. Mineral. Geochem.* **2003**, *53* (1), 63−87.
(31) Cornish-Bowden, A.; Endrenyi, L. Robust regression of enzyme kinetic data. *Biochem. J.* **1986**, *234* (1), 21−0.
(32) Lykourinou, V.; Hanafy, A. I.; Bisht, K. S.; Angerhofer, A.; Ming, L.-J. Iron(III) Complexes of Metal-Binding Copolymers as Proficient Catalysts for Acid Hydrolysis of Phosphodiesters and Oxidative DNA Cleavage − Insight into the Rational Design of Functional Metallopolymers. *Eur. J. Inorg. Chem.* **2009**, *2009* (9), 1199−1207.
(33) Salvio, R.; Casnati, A.; Mandolini, L.; Sansone, F.; Ungaro, R. ATP cleavage by cone tetraguanidinocalix[4]arene. *Org. Biomol. Chem.* **2012**, *10* (45), 8941−8943.
(34) Holbrook, K. A.; Ouellet, L. The non-enzymatic hydrolysis of p-nitrophenyl phosphate. *Can. J. Chem.* **1958**, *36* (4), 686−690.
(35) Zhang, Z. Y.; Malachowski, W. P.; Vanetten, R. L.; Dixon, J. E. Nature of the rate-determining steps of the reaction catalyzed by the yersinia protein-tyrosine-phosphatase. *J. Biol. Chem.* **1994**, *269* (11), 8140−8145.
(36) Gaunt, A. J.; May, I.; Collison, D.; Travis Holman, K.; Pope, M. T. Polyoxometal cations within polyoxometalate anions. Seven-coordinate uranium and zirconium heteroatom groups in $[(UO_2)_{12}(\mu_3\text{-}O)_4(\mu_2\text{-}H_2O)_{12}(P_2W_{15}O_{56})_4]^{32-}$ and $[Zr_4(\mu_3\text{-}O)_2(\mu_2\text{-}OH)_2(H_2O)_4(P_2W_{16}O_{59})_2]^{14-}$. *J. Mol. Struct.* **2003**, *656* (1−3), 101−106.
(37) (a) Jones, D. R.; Lindoy, L. F.; Sargeson, A. M. Hydrolysis of phosphate esters bound to cobalt(III). Kinetics and mechanism of intramolecular attack of hydroxide on coordinated 4-nitrophenyl phosphate. *J. Am. Chem. Soc.* **1983**, *105* (25), 7327−7336. (b) Chin, J.; Banaszczyk, M. Highly efficient hydrolytic cleavage of adenosine monophosphate resulting in a binuclear cobalt(III) complex with a novel doubly bidentate μ^4-phosphato bridge. *J. Am. Chem. Soc.* **1989**, *111* (11), 4103−4105. (c) Deck, K. M.; Tseng, T. A.; Burstyn, J. N. Triisopropyltriazacyclononane copper(II): An efficient phosphodiester hydrolysis catalyst and DNA cleavage agent. *Inorg. Chem.* **2002**, *41* (4), 669−677. (d) Deal, K. A.; Hengge, A. C.; Burstyn, J. N. Characterization of transition states in dichloro(1,4,7-triazacyclononane)copper(II)-catalyzed activated phosphate diester hydrolysis. *J. Am. Chem. Soc.* **1996**, *118* (7), 1713−1718.
(38) (a) Supkowski, R. M.; Horrocks, W. D., Jr On the determination of the number of water molecules, q, coordinated to europium(III) ions in solution from luminescence decay lifetimes. *Inorg. Chim. Acta* **2002**, *340* (0), 44−48. (b) Parker, D. Luminescent lanthanide sensors for pH, pO_2 and selected anions. *Coord. Chem. Rev.* **2000**, *205* (1), 109−130.
(39) (a) Goovaerts, V.; Stroobants, K.; Absillis, G.; Parac-Vogt, T. N. Molecular interactions between serum albumin proteins and Keggin type polyoxometalates studied using luminescence spectroscopy. *Phys. Chem. Chem. Phys.* **2013**, *15* (42), 18378−18387. (b) Goovaerts, V.;

DOI: 10.1021/acs.inorgchem.6b01802
Inorg. Chem. XXXX, XXX, XXX−XXX

Stroobants, K.; Absillis, G.; Parac-Vogt, T. N. Eu(III) luminescence and tryptophan fluorescence spectroscopy as a tool for understanding interactions between hen egg white lysozyme and metal-substituted Keggin type polyoxometalates. *J. Inorg. Biochem.* **2015**, *150*, 72−80.
(40) (a) Vichard, C.; Kaden, T. A. Phosphate and phosphonate ester hydrolysis promoted by dinuclear metal complexes. *Inorg. Chim. Acta* **2002**, *337* (0), 173−180. (b) Shim, H.; Hong, S.-B.; Raushel, F. M. Hydrolysis of Phosphodiesters through Transformation of the Bacterial Phosphotriesterase. *J. Biol. Chem.* **1998**, *273* (28), 17445−17450. (c) Cassano, A. G.; Anderson, V. E.; Harris, M. E. Understanding the transition states of phosphodiester bond cleavage: Insights from heavy atom isotope effects. *Biopolymers* **2004**, *73* (1), 110−129. (d) Sumaoka, J.; Furuki, K.; Kojima, Y.; Shibata, M.; Hirao, K.; Takeda, N.; Komiyama, M. Active Species for Ce(IV)-Induced Hydrolysis of Phosphodiester Linkage in cAMP and DNA. *Nucleosides, Nucleotides Nucleic Acids* **2006**, *25* (4−6), 523−538.
(41) (a) Katada, H.; Seino, H.; Mizobe, Y.; Sumaoka, J.; Komiyama, M. Crystal structure of Ce(IV)/dipicolinate complex as catalyst for DNA hydrolysis. *JBIC, J. Biol. Inorg. Chem.* **2008**, *13* (2), 249−255. (b) Zhao, M.; Zhao, C.; Jiang, X.-Q.; Ji, L.-N.; Mao, Z.-W. Rapid hydrolysis of phosphate ester promoted by Ce(IV) conjugating with a β-cyclodextrin monomer and dimer. *Dalton Trans.* **2012**, *41* (15), 4469−4476.
(42) Duarte, F.; Åqvist, J.; Williams, N. H.; Kamerlin, S. C. L. Resolving Apparent Conflicts between Theoretical and Experimental Models of Phosphate Monoester Hydrolysis. *J. Am. Chem. Soc.* **2015**, *137* (3), 1081−1093.
(43) Sap, A.; De Zitter, E.; Van Meervelt, L.; Parac-Vogt, T. N. Structural Characterization of the Complex between Hen Egg-White Lysozyme and Zr^{IV}-Substituted Keggin Polyoxometalate as Artificial Protease. *Chem. - Eur. J.* **2015**, *21* (33), 11692−11695.
(44) Glasoe, P. K.; Long, F. A. Use of glass electrodes to measure acidities in deuterium oxide. *J. Phys. Chem.* **1960**, *64* (1), 188−190.
(45) Frisch, M. J.; Trucks, G. W.; Schlegel, H. B.; Scuseria, G. E.; Robb, M. A.; Cheeseman, J. R.; Scalmani, G.; Barone, V.; Mennucci, B.; Petersson, G. A.; Nakatsuji, H.; Caricato, M.; Li, X.; Hratchian, H. P.; Izmaylov, A. F.; Bloino, J.; Zheng, G.; Sonnenberg, J. L.; Hada, M.; Ehara, M.; Toyota, K.; Fukuda, R.; Hasegawa, J.; Ishida, M.; Nakajima, T.; Honda, Y.; Kitao, O.; Nakai, H.; Vreven, T.; Montgomery, J. A., Jr.; Peralta, J. E.; Ogliaro, F.; Bearpark, M.; Heyd, J. J.; Brothers, E.; Kudin, K. N.; Staroverov, V. N.; Keith, T.; Kobayashi, R.; Normand, J.; Raghavachari, K.; Rendell, A.; Burant, J. C.; Iyengar, S. S.; Tomasi, J.; Cossi, M.; Rega, N.; Millam, J. M.; Klene, M.; Knox, J. E.; Cross, J. B.; Bakken, V.; Adamo, C.; Jaramillo, J.; Gomperts, R.; Stratmann, R. E.; Yazyev, O.; Austin, A. J.; Cammi, R.; Pomelli, C.; Ochterski, J. W.; Martin, R. L.; Morokuma, K.; Zakrzewski, V. G.; Voth, G. A.; Salvador, P.; Dannenberg, J. J.; Dapprich, S.; Daniels, A. D.; Farkas, O.; Foresman, J. B.; Ortiz, J. V.; Cioslowski, J.; Fox, D. J. *Gaussian 09*, Revision D.01; Gaussian, Inc: Wallingford, CT, 2013.
(46) (a) Becke, A. D. Density-functional thermochemistry. III. The role of exact exchange. *J. Chem. Phys.* **1993**, *98* (7), 5648−5652. (b) Lee, C.; Yang, W.; Parr, R. G. Development of the Colle-Salvetti correlation-energy formula into a functional of the electron density. *Phys. Rev. B: Condens. Matter Mater. Phys.* **1988**, *37* (2), 785−789. (c) Stephens, P. J.; Devlin, F. J.; Chabalowski, C. F.; Frisch, M. J. Ab Initio Calculation of Vibrational Absorption and Circular Dichroism Spectra Using Density Functional Force Fields. *J. Phys. Chem.* **1994**, *98* (45), 11623−11627. (d) Grimme, S.; Antony, J.; Ehrlich, S.; Krieg, H. A consistent and accurate ab initio parametrization of density functional dispersion correction (DFT-D) for the 94 elements H-Pu. *J. Chem. Phys.* **2010**, *132* (15), 154104.
(47) Dolg, M.; Stoll, H.; Preuss, H. Energy adjusted ab initio pseudopotentials for the rare earth elements. *J. Chem. Phys.* **1989**, *90*, 1730.
(48) Hay, P. J.; Wadt, W. R. Ab initio effective core potentials for molecular calculations. Potentials for K to Au including the outermost core orbitals. *J. Chem. Phys.* **1985**, *82*, 299−310.
(49) (a) Cancès, E.; Mennucci, B.; Tomasi, J. A new integral equation formalism for the polarizable continuum model: Theoretical background and applications to isotropic and anistropic dielectrics. *J. Chem. Phys.* **1997**, *107*, 3032−3041. (b) Mennucci, B.; Cancès, E.; Tomasi, J. Evaluation of Solvent Effects in Isotropic and Anisotropic Dielectrics, and in Ionic Solutions with a Unified Integral Equation Method: Theoretical Bases, Computational Implementation and Numerical Applications. *J. Phys. Chem. B* **1997**, *101*, 10506−17.
(50) Weigend, F.; Ahlrichs, R. Balanced basis sets of split valence, triple zeta valence and quadruple zeta valence quality for H to Rn: Design and assessment of accuracy. *Phys. Chem. Chem. Phys.* **2005**, *7*, 3297−3305.
(51) Andrae, D.; Haeussermann, U.; Dolg, M.; Stoll, H.; Preuss, H. Energy-adjusted ab initio pseudopotentials for the second row and third row transition elements. *Theor. Chim. Acta* **1990**, *77*, 123−141.
(52) Neese, F. The ORCA program system. *WIREs Comput. Mol. Sci.* **2012**, *2*, 73−78.
(53) Grimme, S.; Ehrlich, S.; Goerigk, L. Effect of the Damping Function in Dispersion Corrected Density Functional Theory. *J. Comput. Chem.* **2011**, *32* (7), 1456−1465.
(54) (a) Barone, V.; Cossi, M. Quantum calculation of molecular energies and energy gradients in solution by a conductor solvent model. *J. Phys. Chem. A* **1998**, *102*, 1995−2001. (b) Cossi, M.; Rega, N.; Scalmani, G.; Barone, V. Energies, structures, and electronic properties of molecules in solution with the C-PCM solvation model. *J. Comput. Chem.* **2003**, *24*, 669−681.
(55) (a) Pliego, J. R., Jr.; Riveros, J. M. The Cluster-Continuum Model for the Calculation of the Solvation Free Energy of Ionic Species. *J. Phys. Chem. A* **2001**, *105*, 7241−7247. (b) Bryantsev, V. S.; Diallo, M. S.; Goddard, W. A., III Calculation of Solvation Free Energies of Charged Solutes Using Mixed Cluster/Continuum Models. *J. Phys. Chem. B* **2008**, *112*, 9709−9719.

DOI: 10.1021/acs.inorgchem.6b01802
Inorg. Chem. XXXX, XXX, XXX−XXX